Assessment of pH and Temperature Effects on Collagen Gel Microstructure Using Second Harmonic Generation and Scanning Electron Microscopies

By

Ariana Joseph

A Thesis Submitted to
Saint Mary's University, Halifax, Nova Scotia
in Partial Fulfilment of the Requirements for
the Degree of Bachelor of Science with Honours in Biology

April 2020, Halifax, Nova Scotia

Approved: _____
Dr. Danielle Tokarz
Supervisor

Approved: _____
Dr. Anne Dalziel
Examiner

Date: April 10, 2020

Assessment of pH and Temperature Effects on Collagen Gel Microstructure Using Second Harmonic Generation and Scanning Electron Microscopies

by Ariana Joseph

ABSTRACT

Collagen is a fibrous structural protein that possesses a characteristic triple-helical conformation which aids in the stabilisation of molecular confirmations. For example, in tissues collagen aids in maintaining the structural integrity. Collagen accounts for 30% of the total protein content in the body and is a major constituent of the extracellular matrix (ECM). The ECM provides structural support for cellular components and is a key regulator of biochemical functions in the human body related to tissue growth and development. Thus, for the maintenance of normal organ function and to facilitate wound healing, homeostasis of the ECM is crucial. Sustained homeostatic dysregulation results in terminal and pathological conditions such as cancer where structural variation in the ECM is not well understood and is difficult to characterize.

In the current research, natural collagen hydrogels synthesized in differing chemical environments were investigated by second harmonic generation (SHG) and scanning electron microscopies (SEM). The gels were synthesized within biologically relevant ranges of polymerization pH and polymerization temperatures to investigate how these variables affect the structure and morphology of collagen fibrils. Results of imaging dried samples with SEM revealed structural parameters of collagen D-banding periodicity of 59.8 ± 4 nm in gels simulating normal physiological conditions and was in line with the ~67 nm periodicity reported for *in vivo* native-banded fibrils. Qualitative analysis of the hydrogels revealed lower fibril content and thicker fibrils at lower temperatures which was evidenced by higher SHG signals in quantitative analysis. The fibril diameter was maximum at pH 6.5, and lower fibril content was observed at a lower pH. Statistically significant differences were observed in average fibril diameter and in SHG intensities for varied polymerization temperature and pH, demonstrating that the technique can probe collagen microstructure and provide a greater understanding of ultrastructural changes occurring within the ECM.

[April 10, 2020]

ACKNOWLEDGEMENTS

I would like to thank my supervisor, Dr. Danielle Tokarz and her research associate, Dr. Richard Cisek for their expert guidance throughout my undergraduate career, and who shared in the excitement of this past year of discovery. Their unwavering enthusiasm kept me enamoured with my study and fostered my love for creativity and research.

My appreciation also extends to the Tokarz laboratory members, both past and present with special thanks to Katherine P., Kennedy and MacAulay for their suggestions, contributions to this project and for helping to maintain a positive environment for learning science.

To Dr. Anne Dalziel, Dr. Colleen Barber, Dr. David Chiasson and the Honours Class of 2020 for their encouragement, shared curiosity in research and willingness to provide me with feedback every step along the way. I am honoured to have had access to such an enthusiastic support group.

I would like to extend special thanks to both the Chemistry and Biology Departments for the opportunity to contribute positively to the scientific community. To Alyssa Doué, Xiang Yang, Matt Logan, Jing Yang, Carmen Cranley, and Caila Lebans for dealing with my constant requests and any questions I have had along the way.

Lastly, I would like to thank my loved one, family (especially my parents, grandmother and my mom-away-from-home, Julia) and friends for their prayers, understanding, and unwavering support throughout this journey. To you, I will be forever indebted.

TABLE OF CONTENTS

List of Abbreviations:

PDAC	Pancreatic Ductal Adenocarcinoma
ECM	Extracellular Matrix
LOX	Lysol Oxidase
CAF	Cancer Associated Fibroblast
EMT	Epithelial-Mesenchymal Transition
SEM	Scanning Electron Microscopy
SHG	Second Harmonic Generation
PBS	Phosphate-Buffered Saline
dH_2O	Deionized Water
v/v	Volume by Volume (Volume Percent)
APS	Ammonium Persulphate
TEMED	Tetramethylethylenediamine
Fs	Femtosecond
Nm	Nanometre
MHz	Megahertz
NA	Numerical Aperture
HMDS	Hexamethyldisiloxane

List of Tables:

List of Figures:

Introduction

1.1 Motivation

Pancreatic cancer is currently the third- and fourth-leading cause of cancer-related deaths in the United States and Canada respectively (Canadian Cancer Society's Advisory Committee on Cancer Statistics, 2017; Wallis, 2018). The most common malignancy of the pancreas, pancreatic ductal adenocarcinoma (PDAC), retains its status as the deadliest of cancers as it is rarely detected during early stages. It remains asymptotic until metastasis to distant organs (Poruk et al. 2014: Canadian Cancer Society's Advisory Committee on Cancer Statistics, 2018).

Diagnosis of pancreatic cancer poses significant challenge for pathologists as the disease is often characterized by non-specific symptoms, and is dependent upon the availability of major blood vessels around the tumour to support invasion and metastasis (McGuigan et al. 2018). These factors mean that by the time characteristic symptoms have developed, the tumour is at an advanced stage where resection or removal of a section of the pancreas, is no longer feasible (Poruk et al. 2014; McGuigan et al. 2018). Currently, surgical resection is the only plausible cure for PDAC however, remission rates remain relatively high and the rates of long-term survival remain significantly low (Poruk et al. 2014; McGuigan et al. 2018). Owing to the lower incidence rate of PDAC throughout the population compared to other aggressive cancer types, there remains no sensitive screening methods for this cancer in current clinical care (McGuigan et al. 2018).

Although cancer stage remains independent of cancer survival, cancers presented at later stages generally have lower survival rates (Canadian Cancer Society's Advisory

Committee on Cancer Statistics, 2018). Thus, in an effort to improve the prognosis and outcomes of PDAC, the disease and its mechanisms need to be understood on the macro- and microstructural levels to determine strategies for earlier detection and intervention.

Formerly, it was theorized that most cancers resulted from the amassing of somatic mutations in epithelial cells (Bhowmick et al. 2004; Tokarz et al. 2019). Recent studies have built on this theory attributing the tumour microenvironment (inclusive of the extracellular matrix (ECM), blood vasculature, inflammatory cells and fibroblasts) to cancer progression (Tokarz et al. 2019). Specifically, there is reduced oxygenation of tissues which impacts the microenvironment's pH and alters the matrix's structure and function (Roma-Rodrigues et al. 2019). However, two issues pertaining to our understanding of the initiation and proliferation of cancer remain: 1) the chemical factors that give rise to and foster the disease are unclear and, 2) there remains no suitable biological model system in which the interaction of pancreatic cancer cells with matrix proteins, such as collagen can be studied.

1.2 Extracellular Matrix

The growth, development and organization of cells are uniquely coupled to its microenvironment. The ECM is often broadly referred to as the cellular microenvironment; however, the ECM is multifaceted and ordered in an effort to retain the geometric shape and structural integrity of many tissues such as bone, cartilage and basement membranes (Frantz et al. 2010). The ECM also plays a crucial role in the regulation of cell and tissue function and comprises a complex and dynamic array of structural proteins, glycosaminoglycans, glycoproteins and proteoglycans (Frantz et al. 2010; Harjanto et al.

2011). Previously, the ECM functionality was entirely attributed to maintaining structural framework and tissue structure. However, it has recently been found to influence chemical signalling, affecting numerous cellular processes such as cell growth, differentiation, adhesion and migration among others (Frantz et al. 2010).

To maintain normal organ function and to facilitate wound healing, homeostatic regulation of the ECM is important. The scaffold structure of the matrix is maintained through synthesis, secretion and modification and orientation of its components by the cells (Frantz et al. 2010; Cox and Erler 2011). However, sustained homeostatic dysregulation and uncontrolled matrix remodelling can promote the development of terminal and pathological conditions (Cox and Erler, 2011). In particular, ECM remodelling is an essential part of tumour malignancy and metastasis (Figure 2).

The tumour microenvironment is heterogenous, comprising both cellular and acellular components. As collagen is a major component of the ECM, it is a key determinant in the ECM's functional properties (Walker et al. 2018). The proliferation of cancer cells induces changes in ECM architecture and these cells require constant interaction with the ECM (Walker et al. 2018). Specifically, during tumorigenesis there is increased secretion of fibrillar collagens and fibronectin increasing density in the stroma. This is typically accompanied by an increase in

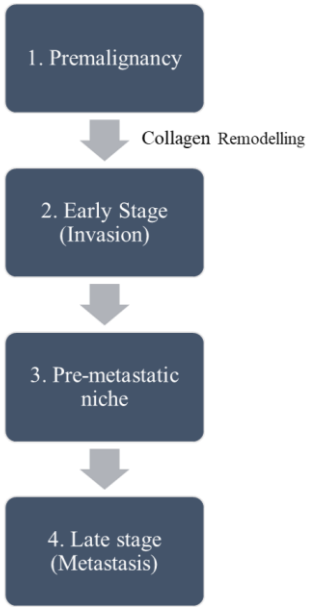

Figure 1: **Schematic of cancer progression**. Figure adapted from Cox and Erler (2011).

LOX cross-linkages increasing ECM stiffness and linearization of collagen fibres responsible for alignment of fibres, and aiding tumour metastasis (Fang et al. 2014; Walker et al. 2018). Despite this knowledge, the specific effects of increased collagen deposition within the ECM associated with cancer progression remains unknown (Walker et al. 2018). Levental et al., (2009) and Karagiannis et al., (2012) identified a correlation between increased collagen cross-linkages and deposition and tumour progression resulting from an increase in integrin signalling by fibroblasts.

1.3Relationship between Pancreatic Tumour Pathology and Collagen

1.3.1 Hallmarks of Pancreatic Collagen

Collagen accounts for one-third of the total protein content in the human body and is the most prevalent structural protein in connective tissue ECM (Gelse et al. 2003; Frantz et al. 2010). Collagen is best defined as a structural glycoprotein containing singular or multiple homologous α chains which possess a triple-helical conformation (Xu et al. 2019). The amino acid sequences of the α chain are characteristically aligned as glycine-X-Y repeats, with X and Y frequently represented by proline and hydroxyproline, although other amino acids may be represented along the length of the chain (Fang et al. 2014; Xu et al. 2019). *In situ* collagen possesses a hierarchal structure (Figure 1; Shoulders and Raines, 2009). Amino acid sequences undergo an assembly mechanism to form large-scale molecular structures which are components of pancreatic tissues (Shoulders and Raines, 2009).

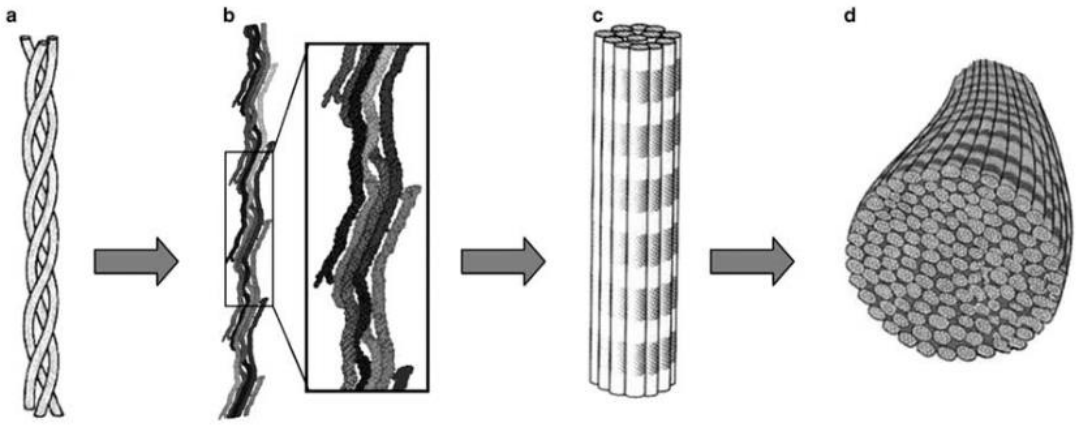

Figure 2: **Characteristic structure of *in situ* collagen: molecule or monomer (a), microfibril (b), fibril with emphasized D-periodicity (c) and fibre (d) during various stages of collagen assembly.** Figure reproduced with permission from Kotova et al. 2015.

The biosynthesis and "self-assembly" of collagen fibres occurs via post translational modification (Lodish et al. 2000). Collagen chains are first synthesized as polypeptide precursors known as procollagens and undergo a series of modifications in the rough endoplasmic reticulum, Golgi apparatus and the extracellular space (Lodish et al. 2000). In the endoplasmic reticulum, the polypeptide chains are glycosylated, hydroxylated and interactions of cysteine residues allow for the formation of interchain disulphide bonds (Lodish et al. 2000). Disulphide bonds between the C-terminus of three procollagens align and initiate triple helical formation towards the N-terminal (Lodish et al. 2000).

Collagen is secreted into the extracellular matrix via exocytosis where it undergoes supramolecular assembly of its fibrils (Lodish et al. 2000; Xu et al. 2019). This may occur following the procollagen cleavage in the transport vesicles (Golgi to membrane carriers) or may occur in the plasma membranes of fibroblasts (Xu et al. 2019). The tensile strength characteristic of collagen fibres is attributed to covalent intra- and inter-molecular Lysol

oxidase (LOX), glycosylation and transglutaminase cross-linkages which differ across collagen (Xu et al. 2019).

In vitro collagen fibril assembly while similar to *in vivo* fibril assembly in that it is a multi-step process, varies largely because of its dependence on environmental variables such as temperature and pH. Gelman et al. (1979) proposed that collagen fibrils synthesized *in vitro* undergo a multi-mechanistic accretion process involving one temperature-independent and two temperature-dependent steps. The first and third processes are temperature-dependent to initiate the formation of an unidentified intermediate and to facilitate lateral growth of the fibrils respectively, while the second is temperature-independent to allow for linear growth of the filaments. These three steps are required for the formation of fibrils which possess similar periodicities and ultrastructural properties to those of *in vivo* fibrils. It is hypothesized that the accretion process enables optimization of the gel microstructure and produces fibrils with increased structural integrity.

Collagen can be classified on the basis of fibrous, non-fibrous and filamentous ultrastructure (Figure 2; Bailey, 1987; Lodish et al. 2000). The former maintains the structural integrity of the fibrils while the latter maintains a degree of tissue flexibility (Lodish et al. 2000). Collagenous structures in the ECM may also be classed as fibrillar, network and transmembrane collagenous domains (Lodish et al. 2000; Gelse et al. 2003; Abraham et al. 2008). There are 28 different types of vertebrate collagen encoded by 42 individual genes which differ in their polypeptide sequences and in their molecular structures and weight (Shoulders and Raines, 2009; Karsdal, 2016; Xu et al. 2019). Among these types, a few of which are highlighted in Table 1, it is mainly collagen types I, III and

V (which are secreted by fibroblasts) and collagen type IV (which is produced by epithelial and endothelial cells) (Xu et al, 2019) that are major components of the ECM.

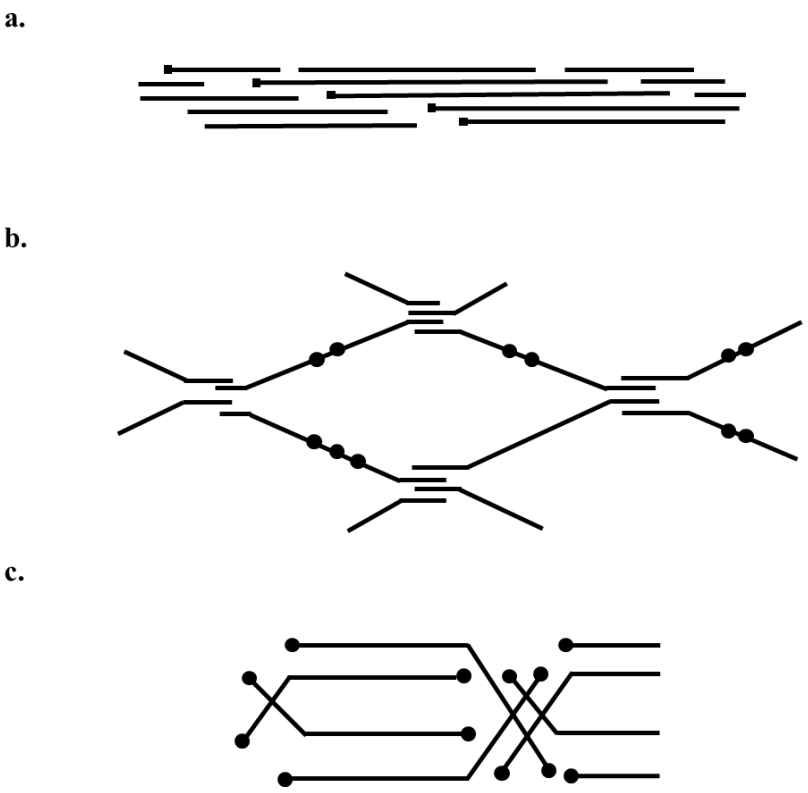

Figure 3: **Supramolecular structures depicted for each collagen classification: fibrous collagens (a), non-fibrous collagens (b) and filamentous collagens (c).** Figure adapted from Figure 1 of Bailey 1987.

Table 1. Predominant Vertebrate Collagen Types, Forms and Distribution.

Collagen Class[1, 3, 4]	**Type**[1, 2, 4]	**Molecular Composition**[1, 2, 3]	**Polymerized Form**[1, 3, 4]	**Tissue Distribution and Composition**[1, 2, 3, 4]	**Structural Details (Monomer Size, Banding Details)** [2]
Fibril-forming	I	$[\alpha1(I)]_2\alpha2(I)$	Fibril	Abundant and widespread: bone, dermis, tendon, ligaments, cornea	300 nm, 67-nm banded fibrils
	II	$[\alpha1(II)]_3$	Fibril	Cartilage, vitreous humour, nucleus pulposus, intervertebral disc	300 nm, 67-nm fibrils
	III	$[\alpha1(III)]_3$	Fibril	Skin, vessel wall, reticular fibres of most tissues (lungs, liver, spleen, etc.); frequently with type I	300 nm, 67-nm fibrils
	V	$[\alpha1(V)]_2\alpha2(V)$ and $\alpha1(V)\alpha2(V)\alpha3(V)$	Fibril (assembly occurs with type I)	Lung, cornea, bone, foetal membranes	390 nm N-terminal globular domain, small fibres
Basement membrane	IV	$[\alpha1(IV)]_2\alpha2(IV)$; $\alpha1$-$\alpha6$	Sheet-like network	Basement membrane	390 nm, C-terminus globular domain, nonfibrillar

[1] Gelse et al. 2003

[2] Abraham et al. 2008

[3] Shoulders and Raines, 2009

[4] Fang et al. 2014

Fibrous collagens (types I, II, III and V) possess a characteristic D-banding periodicity where D ~67nm (Chapman, 1985; Lodish et al. 2000; Shoulder and Raines, 2009). This structure is unique to collagens found in the interstitial matrix and is not characteristic of basement membrane collagen (i.e. type IV collagen; Chapman, 1985).

While some studies credit this periodicity to the displacement of collagen molecules produced from side-by-side interactions (Lodish et al. 2000), others suggest this structural parameter occurs because of gaps and overlaps within the collagen fibril (Shoulder and Raines, 2009). While the molecular origin of this periodicity remains unknown, it is often referred to as D-banding periodicity and manifests in the form of repeated striations or ridges throughout the length of the collagens fibrils which can be visualized using electron microscopy (Chapman, 1985; Lodish et al. 2000).

1.3.2 Vertebrate Collagen Types: I, III, IV, V

Fibril-forming collagens: Types I, III, V

Type I collagen, a fibrillar type collagen, is a major component of connective tissues (Gelse et al. 2003; Karsdal, 2016). It is a key regulator of the structural composition of several fibrous tissue types exclusive of cartilage (Karsdal, 2016). Collagen I is by far the best investigated collagen type and has previously been referred to as the archetypal collagen because of the lack of imperfections associated with its triple-helical structure (Gelse et al. 2003; Shoulders and Raines, 2009; Karsdal, 2016). Type I collagen is the principal protein of the interstitial matrix and is expressed in almost all connective tissues (Karsdal, 2016). Collagen type I is responsible for the desmoplastic reaction in PDAC (Öhlund et al. 2013; Weniger et al. 2018). This reaction is defined as the excessive deposition or growth of stroma within regions of the tumour and occurs because of increased synthesis of ECM proteins by stromal cells such as fibroblasts (DeClerk, 2012). Desmoplastic reactions are responsible for the qualitative and quantitative changes in the ECM, such as disruptions within the basement membrane (Öhlund et al. 2013; Weniger et al. 2018).

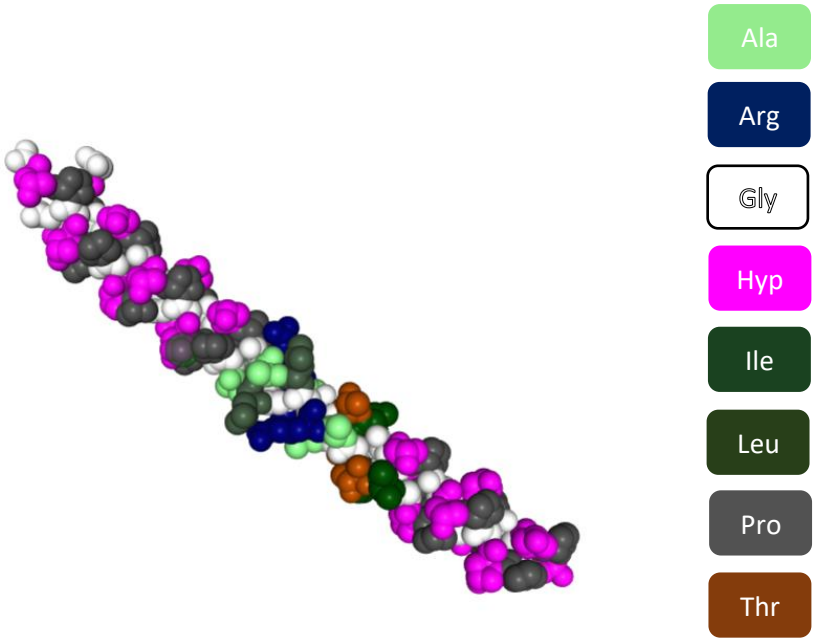

Figure 4: **Molecular Structure of Collagen Type I**. Collagen template adapted from The Protein Data Bank, Protein: 1BKV (Berman et al. 2000). Image was modified using Protein Data Bank Software (Bioassembly 1; spacefilled and coloured by amino acid residue).

Types III and V are both fibrillar type collagens. Type III collagen is often present in type I collagen-containing interstitial matrices and connective tissues such as skin, internal organs and the vascular system (Karsdal, 2016). Type V, on the other hand, is essential in the fibrillation of collagen types I and III (Karsdal, 2016). Specifically, it determines collagen assembly in individual tissues and plays an important role in optimal fibrillar formation and tissue quality (Karsdal, 2016). Karsdal (2016) proposed that type V collagen is integrated into the interior of the fibrils, while type I collagen assembles along the fibril surface.

Basement Membrane Collagen: Type IV

Type IV, on the other hand is a network-forming collagen. It is a major component of the basement membrane, which functions as a barrier between tissue compartments and contains key signalling proteins important for physiological and pathological functions (Karsdal, 2016). Characteristically, collagen IV fibrils have 21-26 interruptions of their Glycine-X-Y repeat which decreases structural rigidity and increases flexibility of the structure for optimal network formation (Karsdal, 2016).

When collagen turnover becomes dysregulated, it tends to promote pathological conditions such as cancer by influencing tumour cell behaviour and immunity (Nissen et al. 2019). Cancer cells also alter collagen forming a reinforcing cell-collagen loop which allows for cancer progression and metastasis (Xu et al., 2019). Although ECM alterations are not well understood, an upregulation of fibrillar collagen types (desmoplasia of types I, III and V) and suppression of basement membrane forming collagens (i.e., type IV) are hallmarks of many cancers inclusive of pancreatic cancer (Nissen et al. 2019). For example, the microstructure of the pancreas during tumefaction is defined by dense regions of collagen I and III bundles and a loss of basement membrane integrity (Öhlund et al. 2013).

1.3.3 Effects of Pancreatic Cancer Growth on Collagen Fibre Architecture

Cancer proliferation and progression results in structural changes within the extracellular matrix (ECM) of cells. During cancer development, the content and integrity of the matrix is altered in order to support the biological and biochemical properties of cancer cells (Xu et al. 2019). Specifically, changes within collagen content and architecture are strongly

influenced by mutations in tumour suppressor genes, proto-oncogenes and G-proteins (Xu et al. 2019).

Collagenous ultrastructure is strongly influenced by the mutated tumour suppressor gene, p53. Under mutant conditions, the p53 pathway is responsible for regulating: 1) collagen bundle alignment 60° to 90° relative to the cancer border (Kenny et al. 2017) and 2) collagen's response to stimulation from pancreatic cancer cells (Xu et al. 2019). Other tumour suppressor genes also play a role in cancer progression. Progression can be controlled via the deletion or silencing of specific genes which results in increased recruitment of cancer-associated fibroblasts (CAFs) and production of the gene responsible for collagen type I synthesis (Jolly et al. 2016; Alvarez-Garcia et al. 2019; Xu et al. 2019).

Mutant proto-oncogenes also interact with collagen to allow for cancer progression and metastasis. In pancreatic cancer, mutant proto-oncogenes such as KRAS work along with the epithelial-mesenchymal transition (EMT) regulator enhancing collagen production by pancreatic cancer cells (Shields et al. 2019).

G protein family receptors such as Rho can alter the alignment of collagen influencing the density of the matrix. In PDAC, Rho-associated protein kinase (ROCK)/ Rho signalling can interact with CAFs to increase collagen type I degradation and regulate tumour cell behaviour with the ECM (Vennin et al. 2017; Xu et al, 2019).

Currently, it remains difficult to study the effects of cancer growth on collagen's structure *in vivo* as these processes usually occur deep within the body and characterization of collagenous tumour-associated architectures can only be accomplished using invasive biopsy techniques (Tilbury and Campagnola, 2015). Thus, collagen gel model systems can

be useful for probing collagen's structure and morphology *in vitro* as the gel's properties can be easily controlled to simulate the microenvironment of interest.

1.4 Collagen Gels as Model Biological Systems

Collagen gels have been studied extensively because of their ability to mimic biological tissues in terms of structure and physiology. The potential of collagen to be reconstituted makes it a suitable biopolymer for studies involving wound repair, drug delivery and both pathological and nonpathological diseases which extensively remodel collagen.

Collagen hydrogels are advantageous in many studies including aging (Hsu et al. 1994), tissue engineering (Chevallay and Herbage, 2000; Gutowska et al. 2001), drug delivery (Wallace and Rosenblatt, 2003), collagen assembly mechanisms (Cheng et al. 2008), wound-healing (Moulin et al. 1996) and cell migration (Even-Ram and Yamanda, 2005; Chen and Liu, 2017). The reason behind their popularity as a suitable model system for research is because of its biocompatibility, immunogenicity, conservation across species, ability to be naturally remodelled by cells and most importantly, its tunability (Zhu and Kaufman, 2014; Chen and Liu, 2017). The versatility of the hydrogel is extremely important when understanding the mechanisms of connective tissue pathology and disease (Zhu and Kaufman, 2014; Chen and Liu, 2017).

Collagen reconstitution is controlled by polymerization conditions which impact polymer aggregation and allow for the creation of gels with varying microstructures (Pavone and Campagnola, 2014). Previous studies have determined that tuneable factors such as collagen concentration, pH, temperature and ionic strength are determinants of polymerization parameters, hydrogel microstructure (Zhu and Kaufman, 2014; Doyle,

2016). However, more recent combined scanning electron microscopy (SEM) and optical microscopy studies have focused on investigating temperature and pH to produce hydrogels with distinct architectures which may be similar to the tumour microenvironment (Raub et al. 2007; Raub et al. 2008; Doyle, 2016) as during cancer progression, there is a significant decrease in the matrix pH (pH ~6.5; Kato et al., 2013; Anemone et al., 2019).

While these variables have major effects on the structural and mechanical properties of the collagen network, these conditions also influence the assembly and organization of fibrils with the gel (Zhu and Kaufman, 2014). Normal polymerization conditions are defined according to physiological conditions (37°C and pH ~7.4) and produce a homogenous and reticular structure with fibrils of small diameter (Raub et al. 2007; Doyle, 2016). However, by probing the pH or gelation temperature dependence of the gel, the structure becomes heterogenous and fibres either increase or decrease in size as the variation in parameters exceeds those of normal physiological conditions (Doyle, 2016). Collagen gels polymerized under varying chemical conditions can produce vastly different microstructures specific to various future studies.

Over the last two decades, light microscopy techniques have been used in combination with novel nonlinear optical microscopies such as second harmonic generation (SHG). This method has proved advantageous as it uses long excitation wavelengths to provide precise resolution required to probe the structures within the ECM with increased accuracy (Tilbury et al. 2015). SHG microscopy is also optimal as the technique does not require the use of extracellular dyes for identification which may alter the structure of the collagenous matrix when heated by the laser (Pavone and Campagnola, 2014). Previous studies have

used SHG imaging for probing the collagenous architecture of PDAC (Tokarz et al. 2019) demonstrating that the technique has the possibility of probing collagen gel ultrastructure, fibril distribution and alignment.

1.5 Introduction to Second Harmonic Generation Microscopy

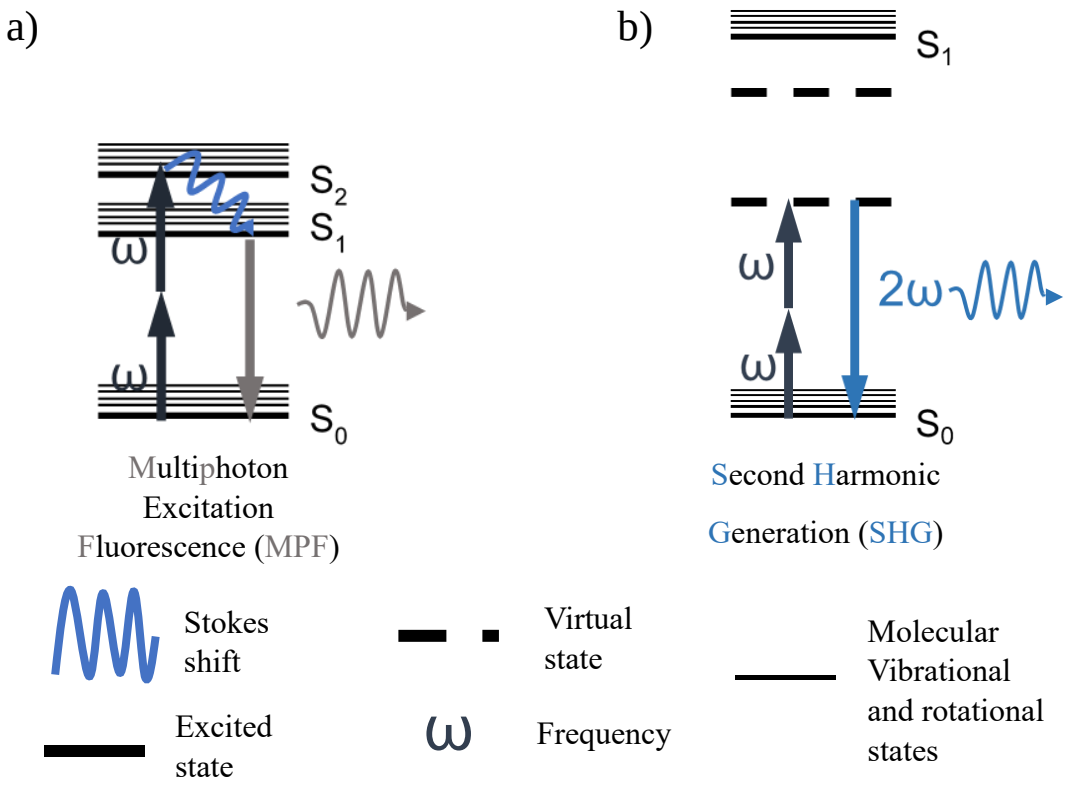

Figure 5: **A comparison between the molecular processes of a) multiphoton excitation fluorescence and b) second harmonic generation** (Boyd, 2008). Figure modified from Tokarz (2014).

Second harmonic generation (SHG) is a non-linear light matter interaction where two photons are converted to one photon. Specifically, SHG is a nonlinear optical phenomenon relying on the hyperpolarizability and non-centrosymmetric properties of a material allowing for discrimination of chiral and nonchiral crystals and noncrystalline aggregates (Hompland et al. 2008). This coherent process produces radiation at twice the frequency

and half the wavelength (Hompland et al. 2008; Campagnola and Dong, 2011; Rouède et al. 2017). Since the photons interact at a virtual state and the excited state is higher than the combined energy of the two photons, molecular absorption of the laser photons does not occur. Unlike fluorescence, there is no molecular absorption and associated Stokes shift, hence this process does not deposit energy into the system (Mohler et al. 2003). As there is no heat production associated with SHG, it has multiple benefits compared to other excitation processes such as fluorescence microscopy, including a reduction in photobleaching and phototoxicity of the sample (Mohler et al. 2003; Hompland et al. 2008). This provides longer duration scans than fluorescence, which can prove advantageous in studies of biological samples. SHG microscopy is also a non-invasive form of microscopy which allows for the study of *in vivo* biological phenomena without the use of dyes as seen in fluorescence microscopy; overcoming a current barrier faced in the advancement of biological research (Mohler et al. 2003). In addition, since SHG microscopy involves the interaction of two photons which leads to a single photon at half of the wavelength, it allows for use of longer wavelengths of light. Longer wavelengths of light results in deeper tissue penetration, another issue associated with using biological imaging techniques (Bueno et al. 2017).

Over the last two decades, SHG microscopy has gained popularity as a unique imaging modality especially with regards to its applications in label-free tissue imaging and *in situ* quantification of fibrillar protein architectures (Rouède et al. 2017). This technique has been well explored with studies ranging from imaging of connective tissues and fibrotic collagen, to imaging of reconstituted collagen structures and actin-myosin complexes

(Campagnola et al. 2002; Chu et al. 2004; Williams et al. 2005; Raub et al. 2007; Campagnola and Dong, 2011; Tokarz et al. 2019).

SHG signal is generated by structures which are noncentrosymmetric (Hompland et al. 2008). Thus, molecules and crystalline structures that lack a centre of symmetry are essential for efficient SHG production and are birefringent (Bueno et al. 2016). The strength of this signal is characterized by the second-order nonlinear optical susceptibility tensor $\chi^{(2)}$ (Hermans et al. 2017). $\chi^{(2)}$ is defined as a non-zero value, where the number of non-zero elements within a material is dependent on asymmetry properties of the molecules or microcrystalline structure of the material (Bueno et al. 2016; Hermans et al. 2017). Biological molecules that are known to produce strong SHG signals include but are not limited to collagen (Cox, 2011; Tokarz et al. 2019), myosin (Campagnola et al. 2002) and polysaccharides such as starch (Cox, 2011; Cisek et al. 2015). Since collagen has a highly ordered molecular arrangement which gives rise to non-centrosymmetric symmetry, it is a suitable candidate for investigation using SHG microscopy (Hompland et al. 2008).

1.6 Objectives

This study focuses on quantitative ultrastructural analysis of collagen structure and morphology under varying chemical conditions to gain a greater understanding of ECM-associated cancer aetiology. Specifically, this project seeks to gain an understanding of how chemical changes in the ECM affect the structure of collagen allowing for the initiation and progression of PDAC.

The objectives of this study are to 1) develop a collagen gel protocol to synthesize acellular hydrogels for study 2) determine the fibrillar structure of collagen in a 3-

dimensional matrix near physiological temperatures and tumour pH, and 3) create a model system specific to SHG studies. By creating a model system through which we can study the morphological changes of collagen fibres, there is a greater ability to deduce the fibrillar structure and arrangement of fibrils produced in a 3-dimensional matrix similar to the ECM. By changing temperature and pH, we hope to determine which extracellular conditions produce the collagen structure and morphology characteristic of PDAC, visualized by SHG microscopy.

2. Materials and Methods

2.1 Synthesizing Collagen Gels

Collagen Type I Gel Preparation:

The procedure used was modified from Raub et al. (2008). Briefly, collagen gels were prepared by mixing the following solutions in order on ice: 20 µL 10× phosphate-buffered saline (PBS) (pH 7.4; consisting of sodium chloride, potassium chloride, sodium phosphate monobasic and potassium dihydrogen phosphate), 11.5 µL dH_2O, 166.7 µL 3.0 mg/ml collagen type I monomer solution from bovine skin (C4243, Sigma Aldrich) and 1.8 µL 1 M sodium hydroxide. Following the addition of the first three solutions, the mixture was vortexed at medium speed four times for 15 seconds to ensure homogeneity of the sample with four 15 second rest periods on ice to prevent the initiation of polymerization after each time it was vortexed. The mixture was then vortexed for another 15 seconds following pH adjustments with either 0.1M or 1 M NaOH to reach the desired pH of 5.5, 6.5, 7.4, 7.5 or 8.5. 20 µL of the mixture was pipetted onto a slide. The sample was subsequently kept in a high humidity container which consisted of a petri dish layered with a moist paper towel at the incubation temperature and sealed with four layers of parafilm. Ensuring high humidity during incubation avoided artefacts due to quick drying, and improved repeatability as well as sample homogeneity. Collagen gels were prepared at a concentration of 2.5 mg/ml, pH 5.5, 6.5, 7.4, 7.5 and 8.5 and the following temperatures: 25°C for 16 hours and 37°C for 40 minutes. Three separately synthesized gel mixtures were made at each condition. In total, 30 gels were made (see table 2). Due to time constraints, only type I collagen was investigated during this study.

Table 2. The number of gels synthesized at the given pH and temperature.

pH / Temperature	5.5	6.5	7.4	7.5	8.5
25°C	3	3	3	3	3
37°C	3	3	3	3	3

2.2 Fibril Detection in Collagen type I Gels

2.2.1 Synthesis of Turmeric Dye:

3.75 mg of milled *Curcuma longa* powder (Organic Earth Market) was weighed and dissolved in 25 ml of 70% volume by volume (v/v) ethanol. The prepared solution was left for 2 hours in a tightly sealed container after which the solution was transferred to test tubes and centrifuged at 3000 rpm for 5 minutes. The supernatant from each tube was removed, combined and stored until use (Figure 6).

Figure 6: **0.15 mg/mL Turmeric Stain**

2.2.2 Experimental Control -Acrylamide Gel Preparation:

Acrylamide gels were synthesized as a negative control to confirm fibril identification within the collagen gels. Encapsulation of the collagen monomers in acrylamide gel inhibits the formation of collagen fibrils and thus, is not expected to be stained or produce birefringence. The gels were prepared by mixing the following components in order: 50µL of 3.0mg/ml collagen type I monomer solution from bovine skin, 20µL of acrylamide mix (consisting of 1.5 g of acrylamide powder, 0.04 g of bisacrylamide powder and 5 mL of water), 5µL Ammonium persulphate (APS) mix (consisting of 0.1 g of APS and 0.9 mL of

water) and 1µL tetramethylethylenediamine (TEMED). The solution was mixed following the addition of the APS mixture and again after the addition of TEMED. Mixture of the solution was carried out by carefully pipetting the solution up and down to prevent the introduction of bubbles to the solution. 20 µL of the solution was quickly pipetted onto a glass slide and allowed to polymerize. Acrylamide gels were prepared at a concentration of 1.97 mg/ml.

2.3 Characterization of Collagen Gels

2.3.1 Second Harmonic Generation Microscopy

The following characterization procedure was completed in a Class 4 laser laboratory and executed according to Laser Safety Policies and Guidelines. Prior to scanning, samples were prepared for microscopy by placing a coverslip on top of the gel following gelation and sealing the slide and coverslip with clear nail polish to keep the gel from drying.

A custom-built nonlinear optical microscope setup, measuring second harmonic generation intensity, was used in the investigation of collagen gels (Figure 7). The imaging system has been previously described and is only briefly described here (Purvis et al., 2019). The excitation source used was a femtosecond (fs) duration pulsed laser (FemtoLux 3, Ekspla) operating at 1030 nanometre (nm) and ~245 fs pulses generated at a repetition rate of 5 megahertz (MHz). Other key components of the microscope included scanning mirrors, microscope objectives and, a polarizer and liquid crystal modulator for complete polarization and linearization of the incoming light beam.

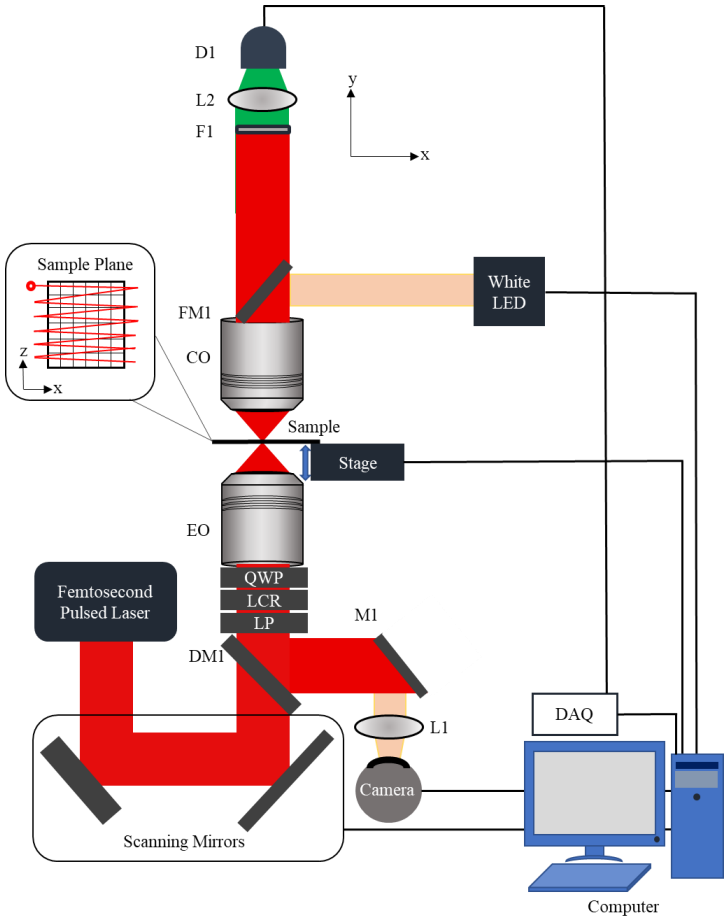

Figure 7: Schematic of the nonlinear optical microscope with the laser traversing the x-y plane. Figure was adapted from Cisek (2012).

Microscope components are as follows: DM: dichroic mirror, M: mirror, FM: flipping mirror, L: optical lenses, F: optical filter, D: photon counting detector, LP: linear polarizer, LCR: liquid crystal retarder, QWP: quarter-wave plate, EO: excitation microscope objective, CO: collection microscope objective, LED: light emitting diode and, DAQ; data acquisition card. The insert on the top left represents the sample plane z-x and the raster scan pattern of laser scanning. Diagram not drawn to scale.

In the experiments, beam focusing was achieved using an excitation microscope objective (Zeiss Apochromat 0.8 numerical aperture (NA) air immersion objective) while signal produced was collected by the collection microscope objective (custom 0.8 NA air objective) in the transmission direction. The aforementioned wavelength and NA resulted

in an axial resolution of approximately 1.5 μm. SHG images were obtained using linearly polarized light to probe the average orientation of the fibrils. Desired polarizations at the focus were achieved using liquid crystal rotators. SHG was isolated using a BG 39 filter (Edmund Optics) and a bandwidth interference filter, (BP 525-25, Edmund Optics) and detected with a photomultiplier tube (H10682-210, Hamamatsu Photonics K.K.) in photon-counting mode. Five to seven images were taken for each of three collagen gels per polymerization temperature and pH.

Image and Data Analysis of SHG images

Prior to analysis, all data was normalized to account for differences in the laser power used for collection. ImageJ (NIH) software was used in the analysis of images acquired by the SHG microscope. The mean and standard deviation of signal intensity per pixel were calculated for each image processed by segmentation which involved finding the maximum value pixel of each signal which contains no distinguishable collagen fibrils. This segmentation excludes void regions so that measurements obtained are only of collagen networks. A noise threshold is set just above this pixel intensity and pixels with signals below this threshold were excluded from the calculations of mean and standard deviation. Segmented images containing <50 pixels were excluded from the calculations. A two-tailed t-test was carried out to test for a significant difference in the fibre intensity within and among gels of varying temperature and pH. P-values were adjusted using the Holm's Sequential Bonferroni Procedure at an alpha level of 0.05. All statistical tests were performed manually in Excel (Microsoft) using standard methods.

2.3.2 Scanning Electron Microscopy (SEM)

Fixation Procedure

The procedure used was modified from Raub et al. (2008). Briefly, collagen gels were prepared for electron microscopy by fixation and serial dehydration. This procedure shrinks and dries the gels, as required for SEM, but preserves the microstructural characteristics produced during polymerization. Following polymerization, collagen gels were fixed with 4% formaldehyde in PBS for 2h at room temperature. After three 5-minute washes in PBS and two 5-minute washes in dH_2O, fixed collagen gels were dehydrated in a graded ethanol/dH_2O series: one 50% v/v, 70% v/v, 95% v/v 10-minute wash and three 100% v/v ethanol 15-minute washes. Following the serial dehydration, samples were chemically dried with a graded hexamethyldisiloxane (HMDS)/ethanol series: 33% v/v, 50% v/v, 66% v/v and three 100% v/v HMDS washes for 15 minutes each. The last HMDS wash was allowed to evaporate in a fume hood overnight. Specimens were kept covered during fixation and drying to prevent contamination of the samples. The gels were cracked into smaller pieces, mounted on SEM sample stages using carbon tape and sputter coated with gold to a thickness of 12-15nm using a Bio-Rad JBS-PS-3 Sputter Coater.

Imaging and Data Analysis of SEM images

Samples were imaged in the Electron Microscopy Centre at Saint Mary's University, Halifax, Nova Scotia. Images were captured using a TESCAN Mira3 LMU scanning electron microscope operating at 15kV. Backscattered electrons were collected at magnifications of 5,000×, 20,000×, 50,000×, 80,000× and 125,000×. SEM images obtained were analysed using ImageJ (NIH) software.

Fibril diameter was measured using the line-drawing function. Diameters were measured by drawing a line across the width of the fibril and calculating the length of the line. All fibrils were selected for measurement if they were in focus and did not have another fibril behind of it. Average fibril diameters were selected to be representative of the entire image. D-banding periodicity was measured using the profile plot function and the width of the peak was determined by drawing a line was drawn from centre to centre of each peak. A two-tailed t-test was carried out to test for a significant difference in the fibril diameter and D-banding periodicities within and among gels of varying temperature and pH. P-values were adjusted using the Holm's Sequential Bonferroni Procedure at an alpha level of 0.05. All statistical tests were performed manually in Excel (Microsoft) using standard methods.

2.3.3 Cross-Polarized Light Microscopy

Prior to staining, samples were fixed in 4% formaldehyde in PBS for 2 hours followed by three 5-minute washes in PBS and two 5-minute washes in dH_2O. The alcoholic extract of *C. longa* was used as a cytoplasmic stain. Fixed samples were covered with 20 µL of the cytoplasmic stain for 5 minutes followed by rinses in dH_2O until the rinse was clear.

Stained gels were viewed and photographed under an Olympus BX41 cross-polarized microscope at 10× and 40× magnification. Images were captured using a PixelLINK PL-B623 camera equipped with PixelLINK Capture OEM software operating on Version 2.3.7.13. For comparison, images were taken in birefringence and non-birefringence mode under similar conditions and were analysed using ImageJ (NIH) software. Average intensity was measured for each image. A two-tailed t-test was carried

out to test for a significant difference in the birefringence within and among gels of varying temperature and pH. P-values were adjusted using the Holm's Sequential Bonferroni Procedure at an alpha level of 0.05. All statistical tests were performed manually in Excel (Microsoft) using standard methods.

3. Results and Discussion

3.1 Determining the presence of collagen fibrils and fibril density using Cross-Polarized Microscopy

To validate the protocol developed in the laboratory, this procedure (Materials and Methods, Section 2.2) was used to determine whether collagen fibrils were being formed within each gel and to see whether the gels could be structurally differentiated from each other using readily available polarization techniques.

While the active staining compound remains unclear, the *C. longa* stain was able to stain the collagen fibrils of the polymerized gel within 5 minutes. Polymerized collagen gels appeared a deep orange colour when viewed under light microscopy confirming the presence of collagen fibril bundles (panels A and B; Figure 8). The control gel of collagen monomers was void of the deep orange colour verifying that only polymerized collagen fibrils were being stained by the dye (panel C; Figure 8). Birefringence of the gels (bottom row; Figure 8) confirmed that collagen fibrils were present in the polymerized gels but not in the control where fibrils were absent.

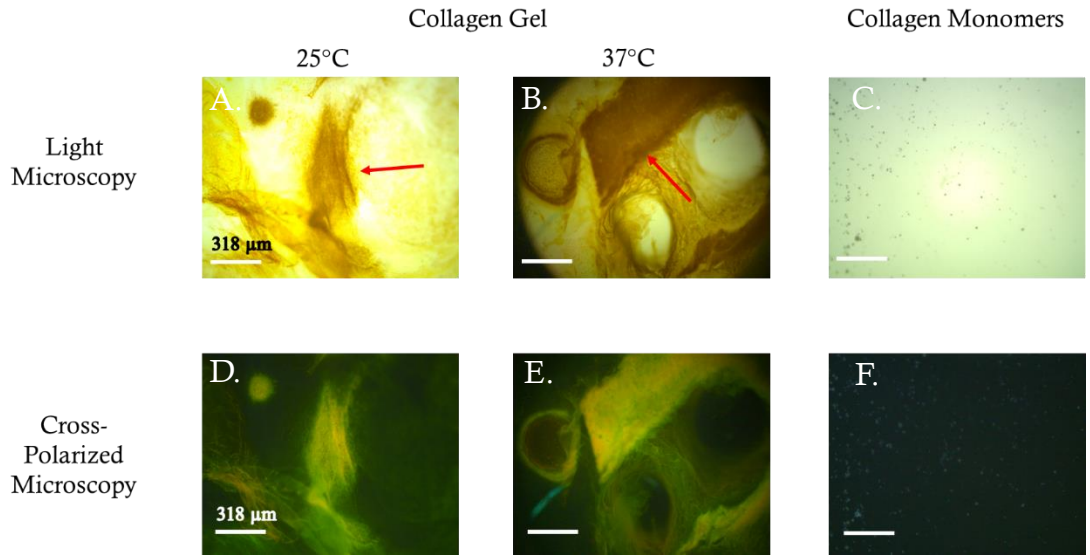

Figure 8: **Photomicrographs of collagen gels showing the staining ability of curcumin and confirming the formation of collagen fibrils**. Representative light microscopy (*top row*) and birefringence (*bottom row*) images of 2.5 mg/mL acellular collagen hydrogels polymerized at pH 7.4 and at 25°C (A, D) and 37 °C (B, E) and 2.5 mg/mL collagen monomers encapsulated in acrylamide gel (C, F). Images are 40×. Ten images were used in intensity quantification and statistical analysis. Red arrows indicated stained collagen fibril bundles within each image. Scale bars are indicated in the figures.

Collagen molecules are highly-ordered molecules with a parallel orientation and thus, produce birefringence (Montes et al. 1984). The dye is acidic in nature and expresses a high affinity for collagen and other basic structures within a cell's cytoplasm such as red blood cells (Avwioro et al. 2007; Kumar et al., 2014). The dye reacts with collagen enhancing the normal birefringence because of the attachment of the dye molecules along their parallel axes (Montes et al. 1984). The significant difference in signal between the polymerized gels and the control ($p<0.003$ for both 25°C and 37°C polymerized gels; Figure 9) could be explained by the presence of fibrils and their localized concentrations within specific sections of the gel. This increases the intensity of the stain within that particular area of the gel. Conversely, the collagen monomers are not polymerized and

remain dispersed throughout the gel, decreasing the signal intensity. The average birefringence for each collagen gel suggests that there may have an increased density of collagen fibrils in collagen gels polymerized at 25°C. While the technique was effective in differentiating average birefringence in gels polymerized at 25°C and 37°C ($p<0.010$), this technique was unable to discriminate specific ultrastructural details of polymerized gels at varying temperatures and highlighted the need for a more sensitive detection system.

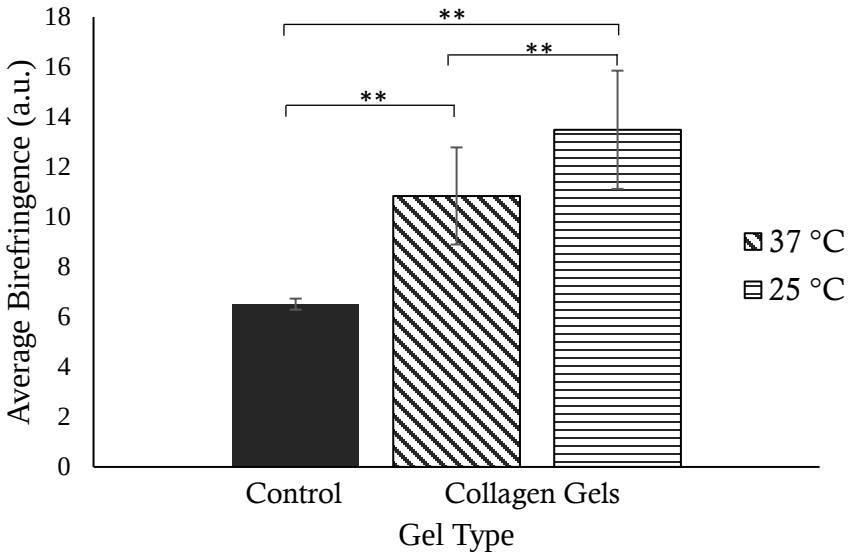

Figure 9: **Average collagen fibril density of 2.5 mg/mL acellular collagen hydrogels and collagen monomers encapsulated in acrylamide gel (control) in arbitrary units (a.u.) as measured by birefringence.** Error bars represent ± one standard deviation. Black bars shown represent the control prepared at room temperature while striped bars represent hydrogels polymerized at 25°C and 37°C. Ten images were used in intensity quantification and statistical analysis. Sample size = 10. A significant difference in average birefringence was found among treatments for control versus 37°C collagen gel ($p<0.003$), control versus 25°C collagen gel ($p<0.003$) and 37°C versus 25°C collagen gels ($p<0.010$). Symbol (**) denotes statistically significant difference among polymerization pH and temperature groups.

3.2 Polymerization temperature and pH effects on gel microstructure

Fibril Morphologies

To determine the effects of polymerization temperature and pH on collagen fibril structure and morphology, synthesized collagen gels were imaged using SEM and SHG microscopy. A reproducible protocol (Materials and Methods, Section 2.1) was developed to study the properties of a large population of collagen type I fibrils within a 3-dimensional matrix. pH 5.5, 6.5, 7.5 and 8.5 were investigated at temperatures of 25°C (for comparison with previous literature results) and 37°C (as this range is near physiological temperature). Different areas of the gel were imaged to provide a representative image of the entire collagen gel. For analysis, fibril diameter was selected as the parameter of study as fibril length was difficult to qualify without disrupting the structure of the entangled fibril network.

Figure 10 shows the collagen gel microstructure as a function of temperature and pH as visualized by SEM. The gel microstructure and collagen fibril morphology varied widely depending on the polymerization pH and temperature. The matrix appears qualitativey tighter at both higher polymerization temperature and pHs (Figure 10). These results are consistent with previous work carried out by Rosenblatt et al. (1994), and Raub et al. (2008). Although it is difficult to directly compare the results of each study, due to difference in methodologies, the general interpretation remains the same: a deviation from physiological pH (pH 7.4) results in increased rigidity within the gel microstructure. This effect may be attributed to the increase in electrostatic interactions between charged residues and resulting in a tighter arrangement of the fibrils and ultimately higher

mechanical properties (Rosenblatt et al. 1994; Raub et al. 2008; Achilli and Mantovani, 2010).

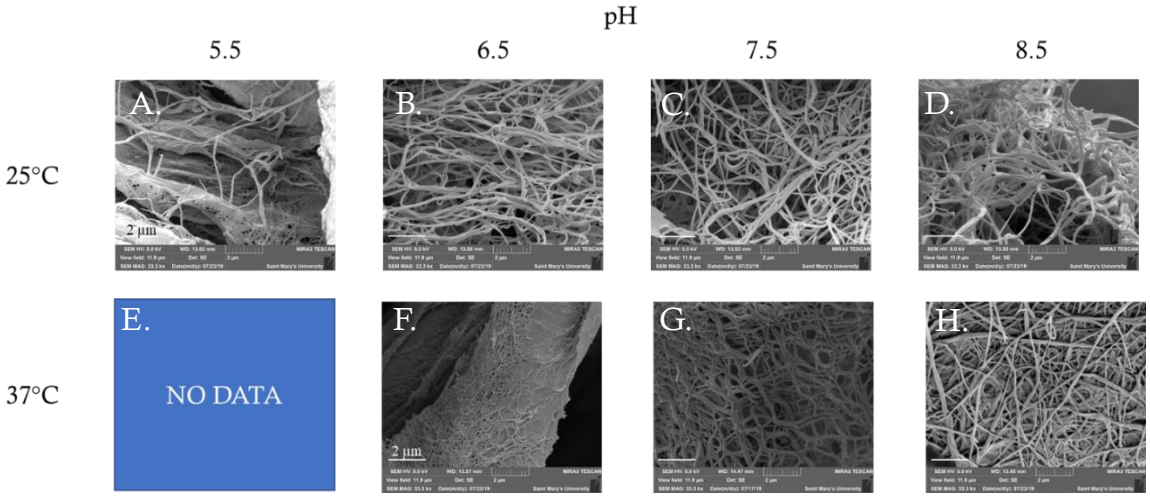

Figure 10: **Representative SEM images of 2.5 mg/mL acellular collagen hydrogels at 25 °C (A-D) 37 °C (E-H) and at pH 5.5, 6.5, 7.5, and 8.5.** Images are 80,000×. Five images were used in microstructure quantification and statistical analysis. The scale bars are indicated in the figures.

Collagen gel networks became more homogenous, reticular and uniform in diameter as the polymerization temperature increased from 25 to 37°C (Figure 10). At higher temperatures, the gel microstructure possesses less fibril bundling than at lower temperatures. These results are consistent with previous work carried out by Raub et al. (2007), Yang et al. (2009), Jansen et al. (2018) and Jones et al. (2014) and can be attributed to kinetics and hydrodynamic effects which alter the heterogeneity of the microstructure and cluster potential of the fibrils (Jones et al. 2014). At lower temperatures, there is a decreased rate of fibril nucleation and thus, a small number of collagen fibrils are able to grow before being cross-linked. Hydrodynamic effects occur because of the motion of water within the gel. These effects result in an increased alignment of the fibrils with one another leading to a heterogenous matrix (Jones et al. 2014). At higher temperatures

however, there is an increased nucleation and growth rate. Thus, the fibrils crosslink before a significant orientational correlation is achieved resulting in a homogenous matrix with shorter and thinner fibrils (Jones et al. 2014).

SEM images also revealed a trend of decreasing fibril diameter with increasing polymerization temperature (Figure 11). This result can be attributed to assembly properties and polymerization kinetics of collagen. Higher temperatures during fibrillogenesis affect the final fibril morphology of collagen by strengthening the electrostatic and hydrophobic interactions and, hydrogen bond forces of collagen monomers. This in turn enhances fibril precipitation in solution and limits lateral aggregation to produce thinner fibrils (Raub et al. 2007; Achilli and Mantovani, 2010).

A similar trend of decreasing fibril diameter was also observed with increasing polymerization pH at 25°C. Data collected at a polymerization temperature of 25°C at pH 5.5 was omitted from analysis as the sample size was too small owing to the lack of fibrils present in the gel network. A decreased fibril diameter with increased pH at 25°C is consistent with previous studies by Wood et al. (1960) and Raub et al. (2008) who demonstrated that smaller fibril diameter is correlated to higher pH values and larger fibril diameter to lower pH values at 25°C and room temperature respectively. This can be explained by an extension of the nucleation phase by decreased pH and temperature which allows for fibril aggregation and the development of thicker fibrils (Sung, 2009). An increase in polymerization pH has been shown to decrease the net positive charge on each collagen monomer by deprotonation of the amino acid side chains within the molecule. Decreasing the positive charge allows for increased hydrogen bonding between the

collagen triple helices and increases the melting temperature of the collagen molecule (Leikin et al. 1995; Morozova and Muthukumar, 2018). This suggests that at lower pH, where decreased bonding attraction and monomer stability correlates with an extended nucleation phase and increased fibril diameter, there is lateral association of the fibrils through increased attractive forces between the fibrils rather than the monomers (Raub et al. 2008). However, at 37°C, there is an opposite trend where the fibril diameter increases with increasing polymerization pH contrary to previous findings by Roeder et al. (2002). This could be attributed to poor execution of the methodology and errors in pipetting leading to incorrect pH values. No data were collected at a polymerization temperature of 37°C and pH 5.5 as fibrils could not be visualized within the gel using SEM.

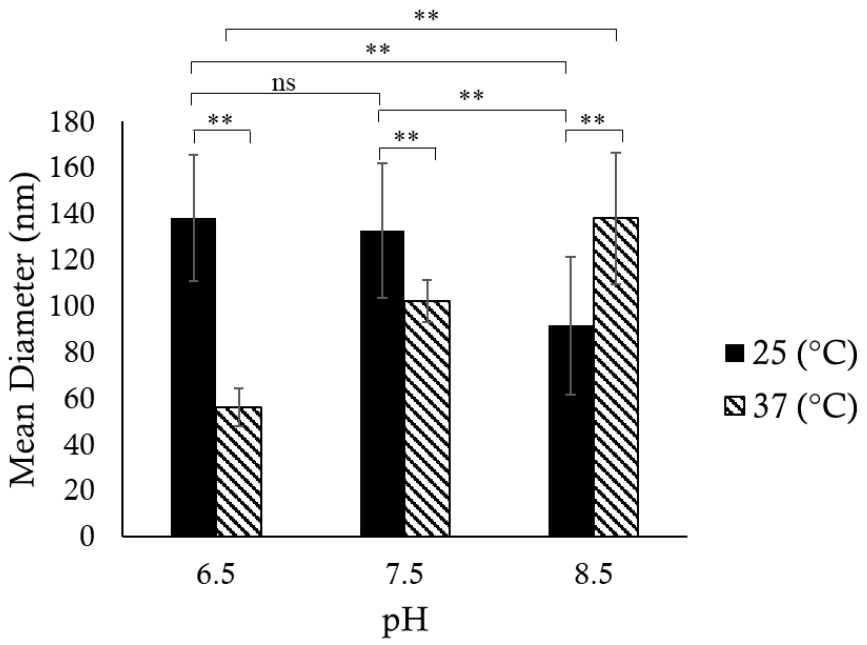

Figure 11: **Mean diameter of collagen fibrils in nm at various pHs and temperatures.** Error bars represent ± one standard deviation. Black bars shown represent gels polymerized at 25°C while striped bars represent hydrogels polymerized at 37°C. Twenty fibrils from five images were used in diameter quantification and statistical analysis. Sample size = 5. A significant difference ($p<0.009$) in mean collagen fibril diameter was determined among

treatments for pH 6.5, 7.5 and 8.5 for 25°C and 37°C polymerized gels. Significant difference ($p<0.009$) was also determined between treatments for pH 6.5 and 8.5 and pH 7.5 and 8.5 for 25°C polymerized gels and pH 6.5, 7.5 and 8.5 for 37°C polymerized gels. No significant difference was found among treatments for pH 6.5 and 7.5 for 25°C polymerized gels ($p<0.50$). Symbols (** and ns) denote a statistically significant difference and no significant difference among polymerization pH and temperature groups, respectively.

Fibrils with periodicities similar to characteristic D-banding periodicity were present in SEM images (Figure 12). Lower pH conditions (pH 5.5 and 6.5) produced gels with a higher proportion of nonfibrillar collagen as such conditions act as inhibitors of fibrillogenesis (Harris and Reiber, 2007). The lower the pH, the more the process of fibrillogenesis is inhibited and a greater amount of nonfibrillar collagen is present within the gel (panels A and F; Figure 10). This demonstrated that under *in vitro* conditions, collagen type I monomers have the ability to form various fibrillar and non-fibrillar assemblies across a wide pH and temperature range in physiological salt conditions.

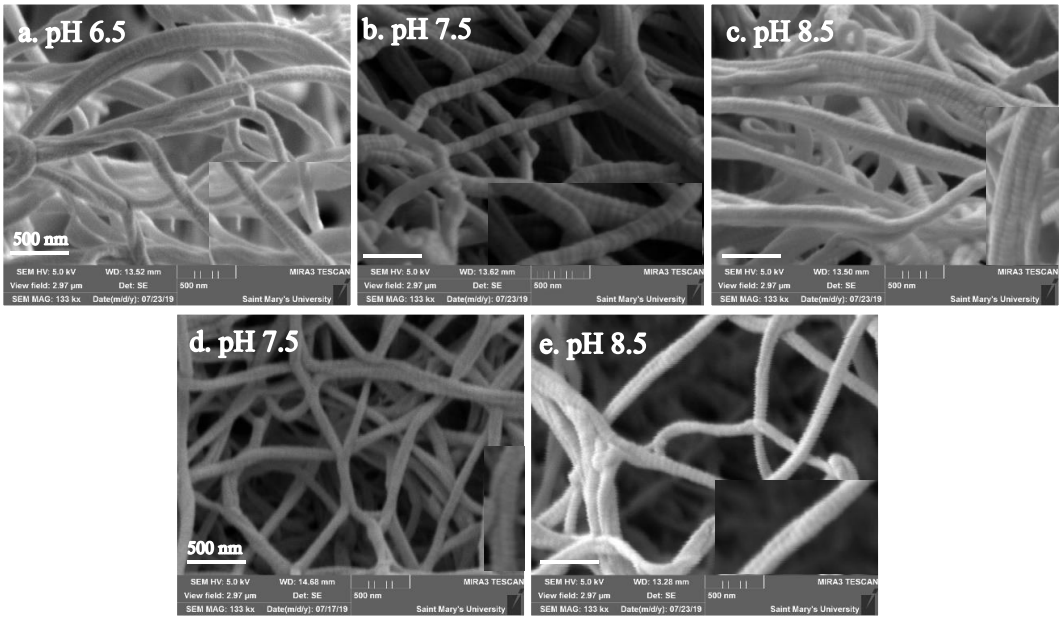

Figure 12: **SEM images of self-assembled collagen fibrils following polymerization at 25°C (a-c) and 37°C (d-e) showing D-banding periodicities.** The insert in the lower right

corner of each image shows a magnified view of a single fibril to emphasize the banding pattern. Images are 80,000×. Three images were used in periodicity quantification and statistical analysis. The scale bars are indicated in the figures.

D-banding Periodicity

Measurement of the D-banding periodicity of self-assembled *in vitro* fibrils is vital as it is believed to play an important role in the mechanical and biological functions of collagenous matrices as well as in mineralization (Glimcher 1959; Fratzl et al. 2004). The D-banding periodicity is characteristic of collagen fibrils and distinguishes them structurally from other fibrils and structures within the matrix (Shoulders and Raines, 2009).

The native-banded fibril is characterized by a D-banding periodicity of 67 nm for *in vivo* tissues (Paige et al., 1998; Shoulders and Raines, 2009) and 64 nm for air-dried samples (Wess and Orgel, 2000). As summarized in Figure 13, the D-banding periodicity in this study was found to range from 46 to 67 nm for pH 6.5, 7.5 and 8.5 (Appendix, Table 3) which is lower than the literature values reported for dehydrated collagen fibrils (Wess and Orgel, 2000). No bands were visualized at the following conditions: pH 5.5 at 25°C and pH 6.5 at 37°C. Holmes et al. (1992), theorized that within the range of physiological pH and salt content, fibrillogenesis produces polymorphic intermediates (sub-fibrils) in the form of early unipolar spindle-shaped D-banded collagen type I fibrils which later fuse together creating the highly-ordered quasi-crystalline collagen fibre structure. Previous work by Gelman et al. (1979) also indicates the conversion of collagen monomers to an intermediate form prior to fibril assembly. This suggests that the D-banding periodicities

observed outside of the reported value may have occurred because of lateral misalignment and ionization-dependence of these sub-fibrils during fibrillogenesis (Harris and Reiber, 2007).

Fibrils retained a periodicity most similar to those of native-banded fibrils when synthesized at a polymerization pH of 8.5 and polymerization temperature of 37°C which is within the range of physiological polymerization conditions: pH 7.4 and 37°C. Retention of the native D-banding periodic structure following reconstitution is crucial as it indicates that the collagen structure being studied is similar to that of *in vivo* collagen. The presence of non-banded fibrils under the conditions: pH 5.5 at 25°C and pH 6.5 at 37°C demonstrated that native banding is subjective under *in vitro* conditions and may be dependent upon the procedure used in fibril reconstitution.

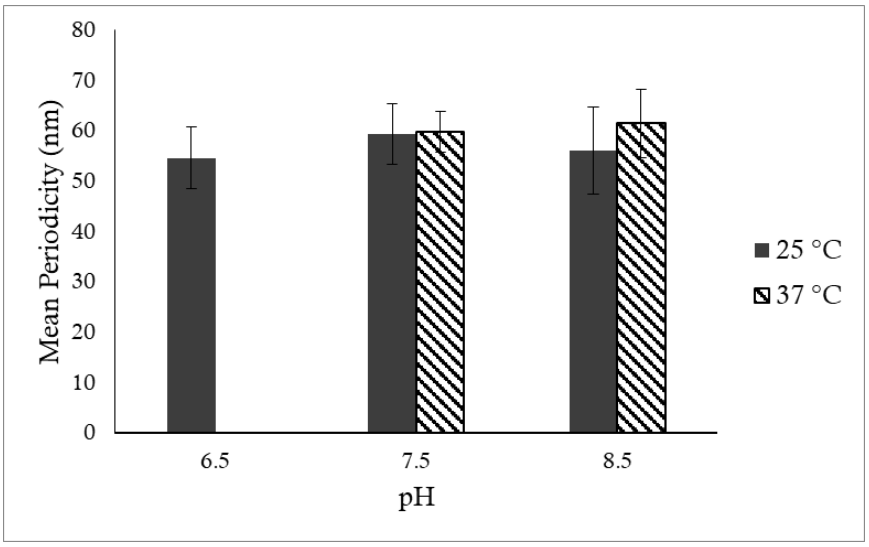

Figure 13: **Mean D-banding periodicity of collagen fibrils in nm at various pHs and temperatures. Error bars represent ± one standard deviation.** Black bars shown represent gels polymerized at 25°C while striped bars represent hydrogels polymerized at 37°C. Ten fibrils from three images were used in periodicity quantification and statistical analysis. Sample size = 10. No significant difference in mean periodicity was determined among treatments for pH 7.5 ($p<1.00$) and pH 8.5 ($p<0.80$) for 25°C and 37°C polymerized

gels. There was also no significant difference between treatments for pH 6.5 and 7.5 ($p<0.50$) and, 6.5 and 8.5 ($p<1.00$) for 25°C polymerized gels and for pH 7.5 and 8.5 ($p<1.00$) for 37°C polymerized gels.

3.3 SHG microscopy of collagen gel microstructure

To date, there has not been clinical application of a non-invasive technique to probe material and organizational properties of the ECM on the cellular scale (Raub et al. 2008; Pinkert et al. 2019). Alterations to the structures within the ECM and ultimately properties of the matrix, such as cancer-associated changes, can have a major impact on the macro- and microscopic biological interactions within the body (Raub et al., 2008). These alterations may not be easily detectable using methods of detection currently employed in clinical care. Thus, this study sought to compare the potential of SHG microscopy, a non-invasive imaging technique, to SEM, an invasive imaging technique, to characterize and discriminate *in vitro* acellular collagen gels for possible use of SHG as a diagnostic tool in the field of histopathology.

Defined microstructural changes were observed between the gels polymerized at different temperatures and pHs and a constant monomer concentration across experiments. Previous SEM assessment revealed a polymerization temperature of 25°C produced dispersed collagenous networks with decreased abundance of thicker fibrils. These fibrils in turn give rise to brighter SHG images with higher SHG intensity values (panels A-D; Figure 14). Contrastingly, hydrogels polymerized at 37°C produced densely-packed collagen meshes containing thinner fibrils at a higher abundance. These fibrils appeared dimmer in SHG images and possessed lower SHG intensities. These characteristics are visible in SHG images of the acellular collagen gels (panels E-H; Figure 14).

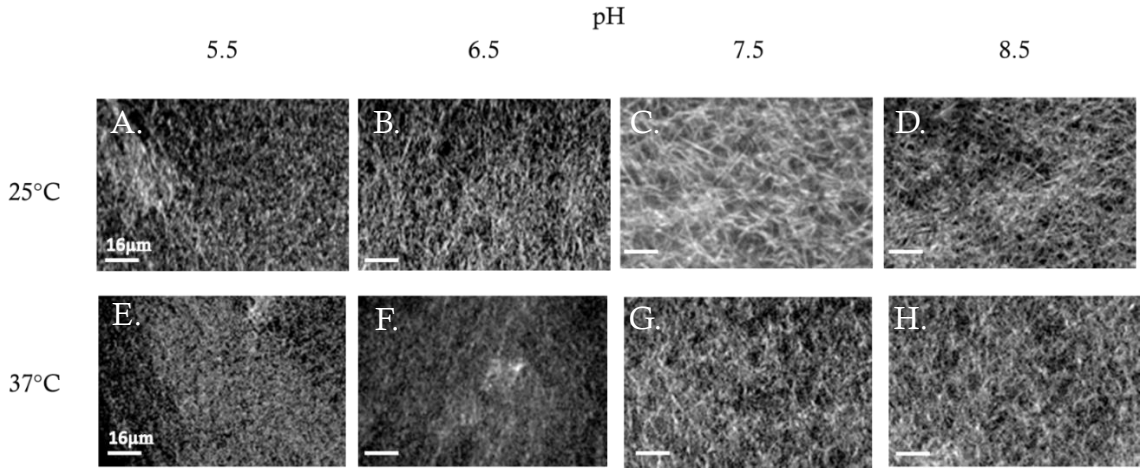

Figure 14: **Representative SHG images of 2.5 mg/mL acellular collagen hydrogels at 25 °C (A-D) 37 °C (E-H) and at pH 5.5, 6.5, 7.5, and 8.5.** Images are 100 × 70 µm. Eleven images were used in microstructure quantification and statistical analysis. The scale bars are indicated in the figures.

Figure 15 shows a substantial decrease in average SHG intensity with increasing polymerization temperature. Decreasing intensity was also observed with increasing polymerization pH at 25°C (Figure 12). However, at 37°C, there is an opposite trend where the average SHG intensity increased with increasing polymerization pH.

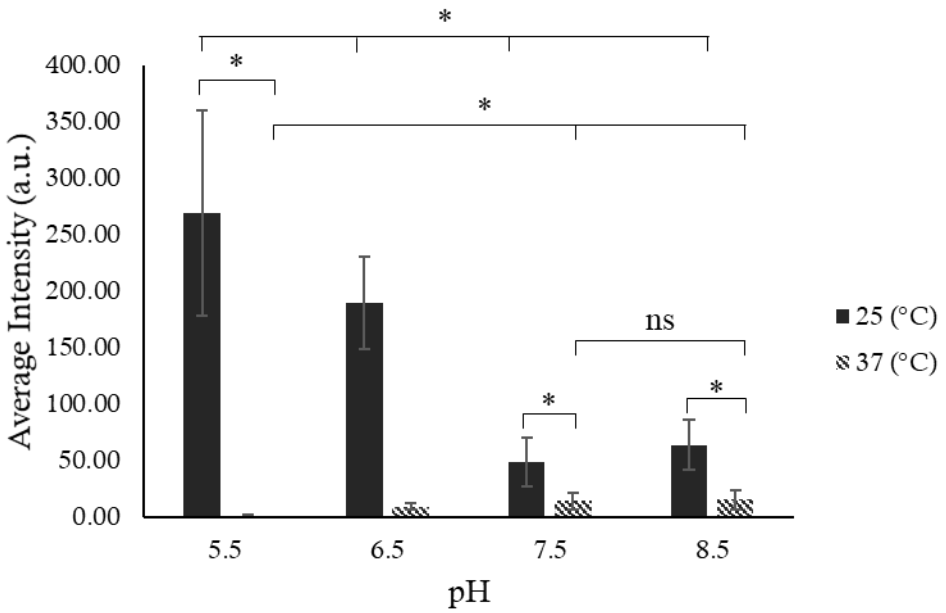

Figure 15: **Average collagen fibril density in counts at varying pH and temperature conditions as measured by SHG intensity. Error bars represent ± one standard deviation.** Black bars shown represent gels polymerized at 25°C while striped bars represent hydrogels polymerized at 37°C. Eleven images were used in intensity quantification and statistical analysis. Sample size = 11. A significant difference in average intensity ($p<0.012$) was determined among treatments for pH 5.5, 7.5 and 8.5 for 25°C and 37°C polymerized gels and between treatments for pH 5.5, 6.5, 7.5 and 8.5 for 25°C polymerized gels and pH 5.5, 7.5 and 8.5 for 37°C polymerized gels. No significant difference was found among treatments for pH 7.5 and 8.5 for 37°C polymerized gels ($p<0.20$). Symbols (* and ns) denote statistically significant difference and no significant difference among polymerization pH and temperature groups, respectively.

Based on the SEM analysis of the polymerized gels, polymerization pH and temperature were found to alter the diameter of the collagen fibrils. This plays an important role in SHG signal transmittance and detection as SHG signals are nonlinearly dependant on the density or thickness of the material (Raub et al. 2008; Pavone and Campagnola, 2014; Fuentes-Corona et al. 2019). In acellular collagen gels, collagen fibrils are the only SHG generating component and (Raub et al. 2008; Pavone and Campagnola, 2014). This suggests that thinner fibrils would give rise to a significant decrease in signal (Fuentes-

Corona et al. 2019), as evidenced in samples polymerized at 37°C and at an increased polymerization pH. Fuentes-Corona et al. (2019) attributes this phenomenon to a decreased concentration of collagen fibrils within the gel to generate SHG signal. However, this explanation is only valid provided the overall fibril concentration and distribution remain unchanged between each sample. Contrastingly, lower polymerization temperatures and lower polymerization pH would be expected to increase the SHG signal generation within the sample as both conditions produce fibrils with increased diameters. Additionally, I speculate that the increased signal observed in gels of lower pHs could be attributed to the higher proportion of non-fibrillar, sheet-like collagen present in these samples, increasing the density of the network within the gels. Increased fibril diameter increases properties of the fibrils favourable for SHG production such as its cross-section and allows for optimum detection (Pavone and Campagnola, 2014). In relation to the trend of increasing intensity at a polymerization temperature of 37°C, the SHG intensity results correspond with the diameters noted in my SEM experiment.

Although my SEM images show a significant difference in diameter of fibrils synthesized at pH 7.5 and 8.5 at 37°C (Figure 11), the result could not be confirmed by the intensity measurement of the fibrils using SHG microscopy since thicker fibrils are expected to produce higher intensities. As the sample is chemically dehydrated for electron microscopy imaging, values for fibril diameter obtained are expected to differ from diameters of native-banded fibres in a hydrated state. Deposition of a metal coating may also affect the thickness of the fibril measured from SEM images, further suggesting that the measured fibril diameter may not be completely accurate (Jansen et al. 2018). While no diameter measurements were calculated from the SHG images obtained, the fibril size

within a gel can be correlated to the SHG signal detected. A similar explanation could be given for the lack of statistical difference in the diameter of hand-measured fibrils synthesized at pH 6.5 and 7.5 at 25°C and the suggestion of fibril size difference based on the intensity measurement of the fibrils within the gels.

In summary, varying the polymerization pH and temperature of collagen gels significantly impacts the overall gel microstructure and the morphology of the collagen fibrils. An increasing pH resulted in thinner collagen fibrils at lower polymerization temperatures with decreased SHG signal intensities and thicker collagen fibrils at higher polymerization temperatures with increased SHG signal intensities. Polymerization temperature and pH were found to have no effect on the D-banding periodicity of the fibrils and reconstituted fibrils were found to be near previously reported physiological periodicities (Paige et al. 1998).

The main contribution of this study was the development and testing of a reproducible hydrogel procedure to probe for changes in collagenous structure using SHG microscopy. Through this study, non-invasive SHG microscopy was combined with invasive SEM imaging, to demonstrated the ability to noninvasively probe hydrogel microstructure and advance the understanding of collagen ultrastructure under conditions of near physiological temperature and tumour microenvironment pH. These data show that SHG microscopy may be a useful histopathological technique to assess and discriminate the structure of collagen within the extracellular matrix of connective tissues affected by PDAC. Integration of SHG into the field of histopathology may allow for earlier detection of PDAC because of the technique's sensitivity to minute structural changes and aid in

increasing the prognosis of the disease. Understanding the specific changes which occur in the extracellular environment that give rise to the cancer-associated collagenous hallmarks can give insight into the mechanism by which these changes occur. With collagenous hallmarks relatively similar across cancer types, obtaining knowledge of collagen content, distribution and macro- and microstructure will give insight into the mechanism and behaviours of other cancer types as well.

4. Future Studies

To further this investigation, the method of synthesis should be retested and adjusted for more precise measurements of the parameters being tested. Rather than manually adjusting the pH of the solution via the addition of an acid or base, specific buffers can be selected with a buffering capacity identical to the pH being tested. This would allow for a more precise pH by preventing the possibility of not obtaining the desired pH. In addition, adapting the current polymerization method for use in a humidity-controlled incubator would negate the need for sealing the sample in a "high-humidity" container, making the process of preparing samples easier and leaving little to no room for human error in terms of ensuring that the temperature within the container is the same as the incubation temperature. This would also decrease the time necessary for sample preparation and could allow for a larger sample size in future work. The procedure can also be improved by imaging the same gel using both SEM and SHG microscopy for a more direct comparison between the two methodologies and their results.

Secondly, future studies should contribute to a further understanding of how the fibrillar assembly and structure of collagen is affected by changes within its chemical environment. Studying the structure of collagen is of great importance as it plays a major role in ECM pathology. In addition to pH and temperature, previous studies have demonstrated several other chemical conditions which not only play a role in cancer initiation and proliferation, but also in gel microstructure and, collagen fibril morphology, alignment and orientation (Achilli and Mantovani, 2010; Lang and Lyubovitsky, 2015). The tumour microenvironment has been found to play a role in maintaining the flux of

sodium and chloride ions to inhibit apoptosis of cancerous cells (Franco et al. 2006; Okada et al. 2006). These ionic species can alter the solubility and thus, the aggregation of proteins suspended within a solution (Achilli and Mantovani, 2010). Thus, collagen should be reconstituted and polymerized in solutions of varying ionic strength to determine their specific effects on collagen fibril structure, morphology and orientation within the gel matrix.

Thirdly, this study also provides the framework for understanding how proteins within the ECM play a role in determining the structure of collagen fibres. Despite collagen type I being the most studied and the most abundant of the collagen types, many other collagen types have been identified as key determinants of matrix stability (Shoulders and Raines, 2009). Karsdal (2016) proposed that fibres within the body are composed of collagen types I, III and V and other ECM proteins which function to regulate the diameter of fibrils and network mechanical properties within tissue. Using the procedure developed, it should be possible to alter the proportion of collagen monomer types within the gel to achieve a structure more similar to that of native collagen fibrils.

Finally, additional measurements such as the arrangement and orientation of collagen fibrils should be determined using polarization-dependent SHG microscopy. Then, SHG can be utilized to its full potential to determine whether the orientation of the fibrils is altered by specific conditions despite similar measurements within other parameters. The microstructure of the gel can be probed in its entirety and collagen's fibril morphology and distribution can then be compared to *in vivo* fibril morphologies present within PDAC histological samples to validate the model system.

5. References

Abraham LC, Zuena E, Perez-Ramirez B, Kaplan DL. 2008. Guide to collagen characterization for biomaterial studies. J Biomed Mat Resear Part B – App Biomater 87B:264-285.

Achilli M, Mantovani D. 2010. Tailoring Mechanical Properties of Collagen-Based Scaffolds for Vascular Tissue Engineering: The Effect of pH, Temperature and Ionic Strength on Gelation. Polymers. 2(4): 664-680.

Ajeti V, Ndiarnykh O, Ponik SM, Keely PJ, Eliceiri KW, Campagnola PJ. 2011. Structural changes in mixed Col I/Col V collagen gels probed by SHG microscopy: implications for probing stromal alterations in human breast cancer. Biomed Opt Express. 2 (8): 2307-2316.

Alvarez-Garcia V, Tawil Y, Wise HM, Leslie NR. 2019. Mechanisms of PTEN loss in cancer: It's all about diversity. Semin Cancer Biol. 59: 66-79.

Anemone A, Consolino L, Arena F, Capozza M, Livo Longo D. 2019. Imaging tumor acidosis: a survey of available techniques for mapping *in vivo* tumor pH. Cancer Metastasis Rev. 38: 25-39.

Avwioro OG, Onwuka SK, Moody JO, Agbedahunsi JM, Oduola T, Ekpo OE, Oladele AA. 2007. Curcuma longa extract as a histological dye for collagen fibres and red blood cells. J Anat. 210 (5): 600-603.

Bailey AJ. 1987. Structure, Function and Ageing of the Collagens of the Eye. Eye. 1: 175-183.

Berman HM, Westbrook J, Feng Z, Gilliland G, Bhat TN, Weissig H, Shindyalov IN, Bourne PE. 2000. The Protein Data Bank. Nucleic Acids Research. 28:235-242.

Bhowmick NA, Neilson EG, Moses HL. 2004. Stromal fibroblasts in cancer initiation and progression. Nature 432: 332-337.

Boyd R. 2008. Nonlinear Optics, 3rd ed. Burlington: Academic Press.

Bueno JM, Ávila FJ, Artal P. 2016. Second Harmonic Generation Microscopy: A Tool for Quantitative Analysis of Tissues. In: Stanciu SG, editor. Microscopy and Analysis. InTech. p2-23.

Bueno JM, Ávila FJ, Artal P. 2017. Comparison of second harmonic microscopy images of collagen-based ocular tissues with 800 and 1045 nm. Biomed Opt Express. 8(11): 5065-5074.

Campagnola PJ, Dong CY. 2011. Second harmonic generation microscopy: principles and applications to disease diagnosis. Laser Photonics Rev. 5(1): 13-26.

Campagnola PJ, Millard AC, Terasaki M, Hoppe PE, Malone CJ, Mohler WA. 2002. Three-Dimensional High-Resolution Second- Harmonic Generation Imaging of Endogenous Structural Proteins in Biological Tissues. Biophys J. 81: 493-508.

Canadian Cancer Society's Advisory Committee on Cancer Statistics. 2017. Canadian Cancer Statistics 2017 – Special topic: Pancreatic cancer. Canadian Cancer Society.

Chapman JA. 1985. The Banding Pattern of Collagen. In: Bairati A, Garrone R, editors. Biology of Invertebrate and Lower Vertebrate Collagens. New York: Plenum Press. p. 515-537.

Chen F, Liu X. 2017. Advancing biomaterials of human origin for tissue engineering. Prog Polym Sci. 53: 86-168.

Cheng X, Gurkan UA, Dehen CJ, Tate MP, Hillhouse HW, Simpson GJ. 2008. An electrochemical fabrication for the assembly of anisotropically oriented collagen bundles. Biomater. 29(22): 3278-3288.

Chevallay B, Herbage D. Collagen-based biomaterials as 3D scaffold for cell cultures: applications for tissue engineering and gene therapy. Med Biol Eng Comput. 38(2): 211-218.

Cisek R. 2012. Structural Investigation of Biological and Semiconductor Nanostructures with Nonlinear Multicontrast Microscopy [dissertation]. [Mississauga (ON)]: University of Toronto.

Chu S, Chen S, Chen G, Tsai T, Chen Y, Lin B, Sun C. 2004. Studies of $\chi^{(2)}/\chi^{(3)}$ Tensors in Submicron-Scaled Bio-Tissues by Polarization Harmonics Optical Microscopy. Biophys J. 86: 3914-3922.

Cisek R, Tokarz D, Steup M, Tetlow IJ, Emes MJ, Hebelstrup KH, Blennow A, Barzda V. 2015. Second harmonic generation microscopy investigation of the crystalline ultrastructure of three barley starch lines affected by hydration. Biomed Opt Express. 6: 3694-3700.

Cox G. 2011. Biological applications of second harmonic imaging. Biophys Rev. 3: 131.

Cox TR, Erler JT. 2011. Remodeling and homeostasis of the extracellular matrix: implications for fibrotic diseases and cancer. Dis Model Mech. 4: 165-178.

DeClerk YA. 2012. Desmoplasia: A Response or Niche? Cancer Discov. 2(9): 772-774.

Doyle AD. 2016. Generation of 3D collagen gels with controlled, diverse architectures. Curr Protoc Cell Biol. 72: 10.20.1-10.20.16.

Ellis H. 2007. Anatomy of the pancreas. Surgery (Oxford). 25: 72-73.

Even-Ram S, Yamanda KM. Cell migration in 3D matrix. Curr Opin Cell Biol. 17(5): 524-532.

Fang M, Yuan J, Peng C, Li Y. 2014. Collagen as a double-edged sword in tumor progression. Tumour Biol. 35: 2871-2882.

Franco R, Bortner CD, Cidlowski JA. 2006. Potential roles of electrogenic ion transport and plasma membrane depolarization in apoptosis. J Membr Biol. 209: 43–58.

Frantz C, Stewart KM, Weaver VM. 2010. The extracellular at a glance. J Cell Sci. 123: 4195-4200.

Fratzl P, Gupta HS, Paschalis EP, Roschger P. 2004. Structure and mechanical quality of the collagen-mineral nano-composite in bone. J Mater Chem. 14(14): 2115-2123.

Fuentes-Corona CG, Licea-Rodriguez J, Younger R, Rangel-Rojo R, Potma EO, Rocha-Mendoza I. 2019. Second harmonic generation signal from type I collagen fibrils grown *in vitro*. Biomed Opt Express. 10(12): 6449-6461.

Gelse K, Pöschl E, Aigner T. 2003. Collagens – structure, function, and biosynthesis. Adv Drug Deliv Rev. 55: 1531-1546.

Gelman RA, Williams BR, Piez KA. 1979. Collagen Fibril Formation: Evidence for a Multistep Process. J Biol Chem. 254(1): 180-186.

Glimcher MJ. 1959. Molecular Biology Of Mineralized Tissues With Particular Reference To Bone. Rev Mod Phys. 31(2): 359-393.

Gutowska A, Jeong B, Jasionowski M. 2001. Injectable gels for tissue engineering. Anat Rec. 263(4): 342-349.

Harjanto D, Maffei JS, Zaman MH. 2011. Quantitative Analysis of the Effect of Cancer Invasiveness and Collagen Concentration on 3D Matrix Remodelling. PLoS One. 6: e24891.

Harris JR, Reiber A. 2007. Influence of Saline and pH on Collagen Type I Fibrillogenesis in Vitro: Fibril Polymorphism and Colloidal Gold Labelling. J Micron. 38(5): 513-521.

Hermans A, Kieninger C, Koskinen K, Wickberg A, Solano E, Dendooven J, Kauranen M, Clemmen S, Wegener M, Koos C, Baets R. 2017. On the determination of $\chi^{(2)}$ in thin films:

a comparison of one-beam second-harmonic generation measurement methodologies. Sci Rep. 7:44581.

Holmes DF, Chapman JA, Prockop DJ, Kadler KE. 1992. Growing tips of type I collagen fibrils formed in vitro are near-parabolic in shape, implying a reciprocal relationship between accretion and diameter. Proc Natl Acad Sci U.S.A. 89: 9855–9859.

Hompland T, Erikson A, Lindgren M, de Lange Davies C. 2008. Second-harmonic generation in collagen as a potential cancer diagnostic parameter. J Biomed Optics. 13: 054050.

Hsu S, Jamieson AM, Blackwell J. 1994. Viscoelastic Studies of Extracellular Matrix Interactions in a Model Native Collagen Gel System. Biorheology. 31(1): 21-36.

Jansen KA, Licup AJ, Sharma A, Rens R, MacKintosh FC, Koenderink GH. The Role of Network Architecture in Collagen Mechanics. Biophys J. 114(11): 2665-2678.

Jolly LA, Novitskiy S, Owens P, Massoll N, Cheng N, Fang W, Moses HL, Franco AT. 2016. Fibroblast-mediated collagen remodeling within the tumor microenvironment facilitates progression of thyroid cancers driven by BrafV600E and Pten loss. Cancer Res. 76:1804–1813.

Jones CAR, Liang L, Lin D, Jiao Y, Sun B. 2014. The spatial-temporal characteristics of type I collagen-based extracellular matrix. Soft Matter. 10(44): 8855–8863.

Karagiannis GS, Poutahidis T, Erdman SE, Kirsch R, Riddell RH, Diamandis EP. 2012. Cancer-associated fibroblasts drive the progression of metastasis through both paracrine and mechanical pressure on cancer tissue. Mol. Cancer Res. 10: 1403–1418.

Karsdal MA, editor. 2016. Biochemistry of Collagens, Laminins and Elastin. United Kingdom: Elsevier.

Kato Y, Ozawa S, Miyamoto C, Maehata Y, Suzuki A, Maeda T, Baba Y. 2013. Acidic extracellular microenvironment and cancer. Cancer Cell Int. 13: 89.

Kenny TC, Schmidt H, Adelson K, Hoshida Y, Koh AP, Shah N, Mandeli J, Ting J, Germain D. 2017. Patient-derived interstitial fluids and predisposition to aggressive sporadic breast cancer through collagen remodeling and inactivation of p53. Clin Cancer Res. 23: 5446–5459.

Kotova SL, Timashev PS, Guller AE, Shekhter AB, Misurkin PI, Bagratashvili VN, Solovieva AB. 2015. Collagen Structure Deterioration in the Skin of Patients with Pelvic Organ Prolapse Determined by Atomic Force Microscopy. Microsc. Microanal. 21(2): 324-333.

Kumar S, Singh NN, Singh A, Singh N, Sinha RK. 2014. Use of Curcuma Longa L. Extract to Stain Various Tissue Samples for Histological Studies. Ayu. 35(4): 447-451.

Lang X, Lyubovitsky JG. 2015. Structural dependency of collagen fibers on ion types revealed by *in situ* second harmonic generation (SHG) imaging method. Anal. Methods. 7(5): 1680-1690.

Leikin S, Parsegian VA, Yang WH, Walrafen GE. 1997. Raman spectral evidence for hydration forces between collagen triple helices. Proc Natl Acad Sci U.S.A. 94(21): 11312-11317.

Levental KR, Yu H, Kass L, Lakins JN, Egeblad M, Erler JT, Fong SF, Csiszar K, Giaccia A, Weninger W, et al. 2009. Matrix crosslinking forces tumor progression by enhancing integrin signaling. Cell. 139: 891–906.

Lodish H, Berk A, Zipursky SL. 2000. Molecular Cell Biology. 4th ed. New York: W.H. Freeman.

Mahadevan V. 2019. Anatomy of the pancreas and spleen. Surgery. 37: 297-301.

McGuigan A, Kelly P, Turkington RC, Jones C, Coleman HG, McCain RS. 2018. Pancreatic cancer: A review of clinical diagnosis epidemiology, treatment and outcomes. World J Gastroenterol. 24(43): 4846-4861.

Mohler W, Millard AC, Campagnola PJ. 2003. Second harmonic generation imaging of endogenous structural proteins. Methods. 29(1): 97-109.

Montes GS, Cotta-Pereira G, Junqueira LCU. 1987. The Connective Tissue Matrix of the Vertebrate Peripheral Nervous System. In: Fedoroff S, editor. Advances in Cellular Neurobiology. Orlando: Academic Press Inc. p. 177-218.

Morozova S, Muthukumar M. 2018. Electrostatic effects in collagen fibril formation. J Chem Phys 149(16): 163333.

Moulin V, Castilloux G, Jean A, Garrel DR, Auger FA, Germain L. 1996. In vitro models to study wound healing fibroblasts. Burns. 22(5): 359-362.

Nissen NI, Karsdal M, Williumsen N. 2019. Collagens and Cancer associated fibroblasts in the reactive stroma and its relation to Cancer biology. J Exp Clin Cancer Res. 38: 115.

Öhlund D, Franklin O, Lundberg E, Lundin C, Sund M. 2013. Type IV collagen stimulates pancreatic cancer cell proliferation, migration, and inhibits apoptosis through an autocrine loop. BMC Cancer. 13:154.

Okada Y, Shimizu T, Maeno E, Tanabe S, Wang X, Takahashi N. 2006. Volume-sensitive chloride channels involved in apoptotic volume decrease and cell death. J Membr Biol. 209: 21–29.

Paige MF, Rainey JK, Goh MC. 1998. Fibrous Long Spacing Collagen Ultrastructure Elucidated by Atomic Force Microscopy. Biophys. J. 74: 3211-3216.

Pavone FS, Campagnola PJ. 2014. Second Harmonic Generation Imaging. Florida: Taylor & Francis.

Pinkert MA, Hortensius RA, Ogle BM, Eliceiri KW. 2018. Imaging the Cardiac Extracellular Matrix. 1098: 21-44.

Poruk KE, Firpo MA, Adler DG, Mulvihill SJ. 2013. Screening for Pancreatic Cancer: Why, How, and Who? Ann Surg. 257(1): 17-26.

Purvis K, Brittain K, Joseph A, Cisek R, Tokarz D. 2019. Third-order nonlinearoptical properties of phycobiliproteins from cyanobacteria and red algae. Chem Phys Lett. 731: 136599.

Raub CB, Suresh V, Krasieva T, Lyubovitsky J, Mih JD, Putnam AJ, Tromberg BJ, George SC. 2007. Noninvasive assessment of collagen gel microstructure and mechanics using multiphoton microscopy. Biophys J. 92:2212–2222.

Raub CB, Unruh J, Suresh V, Krasieva T, Lindmo T, Gratton E, Tromberg BJ, George SC. 2008. Image Correlation Spectroscopy of Multiphoton Images with Collagen Mechanical Properties. Biophys J. 94: 2361-2373.

Roeder BA, Kokini K, Sturgis JE, Robinson JP, Voytik-Harbin SL. 2002. Tensile Mechanical Properties of Three-Dimensional Type I Collagen Extracellular Matrices with Varied Microstructure. *J.* Biomed. Eng. 124: 214–222.

Roma-Rodrigues C, Mendes R, Baptista PV, Fernandes AR. 2019. Targeting Tumour Microenvironment for Cancer Therapy. Int. J. Mol. Sci. 20(4): 840.

Rosenblatt J, Devereux B, Wallace DG. 1994. Injectable Collagen as a pH-Sensitive Hydrogel. Biomater. 15: 985–995.

Rouède D, Schaub E, Bellanger JJ, Ezan F, Scimeca JC, Baffet G, Tiaho F. 2017. Determination of extracellular matrix collagen fibril architectures and pathological remodeling by polarization dependent second harmonic microscopy. Sci Rep. 12197.

Shields MA, Ebine K, Sahai V, Kumar K, Siddiqui K, Hwang RF, Grippo PJ, Munshi HG. 2013. Snail cooperates with KrasG12D to promote pancreatic fibrosis. Mol Cancer Res. 11:1078–1087.

Shoulders MD, Raines RT. 2009. Collagen Structure and Stability. Annu Rev Biochem. 78: 929-958.

Sung KE, Su G, Pehlke C, Trier SM, Eliceiri KW, Keely PJ, Friedl A, Beebe DJ. 2009. Control of 3-dimensional collagen matrix polymerization for reproducible human mammary fibroblast cell culture in microfluidic devices. Biomater. 30(27):4833–4841.

Tilbury K, Lien C, Chen S, Campagnola PJ. 2014. Differentiation of Col I and Col III Isoforms in Stromal Models of Ovarian Cancer by Analysis of Second Harmonic Generation Polarization and Emission Directionality. Biophys J. 106(2): 354-365.

Tilbury K, Campagnola PJ. 2015. Applications of Second-Harmonic Generation Imaging Microscopy in Ovarian and Breast Cancer. Perspect Medicin Chem. 7: 21-32.

Tokarz D. 2014. Nonlinear Optical Properties of Carotenoid and Chlorophyll Harmonophores [dissertation]. [Mississauga (ON)]: University of Toronto.

Tokarz D, Cisek R, Joseph A, Golaraei A, Mirsanaye K, Krouglov S, Asa S, Wilson BC, Barzda V. 2019. Characterization of Pancreatic Cancer Tissue using Multiphoton Excitation Fluorescence and Polarization-Sensitive Harmonic Generation Microscopy. Front Oncol. 9: 272.

Vennin C, Chin VT, Warren SC, Lucas MC, Herrmann D, Magenau A, Melenec P, Walters SN, Del Monte-Nieto G, Conway JR, et al. 2017. Transient tissue priming via ROCK inhibition uncouples pancreatic cancer progression, sensitivity to chemotherapy, and metastasis. Sci Transl Med. 9(384): eaai8504.

Walker C, Mojares E, Del Río Hernández A. 2018. Role of extracellular matrix in development and cancer progression. Int J Mol Sci. 19: 3028.

Wallace DG, Rosenblatt J. 2003. Collagen gel systems for sustained delivery and tissue engineering. Adv Drug Deliv Rev. 55(12): 1631-1649.

Wallis C. 2018. Why Pancreatic Cancer is on the Rise? Sci Am.

Weniger M, Honselmann KC, Liss AS. 2018. The extracellular matrix and pancreatic cancer: A complex relationship. Cancers (Basel). 10: 316.

Wess TJ, Orgel JP. 2000. Changes in Collagen Structure: Drying, Dehydrothermal Treatment and Relation to Long Term Deterioration. Thermochimica Acta. 365:119-128.

Williams RM, Zipfel WR, Webb WW. 2005. Interpreting Second-Harmonic Gneration Images of Collagen I Fibrils. Biophys J. 88: 1377-1386.

Wood GC. 1960. The Formation of Fibrils from Collagen Solutions. A Mechanism of Collagen-Fibril Formation. Biochem. J. 75: 598–605.

Xu S, Xu H, Wang W, Li S, Li H, Li T, Zhang W, Yu X, Liu L. 2019. The role of collagen in cancer: from bench to bedside. J Transl Med. 17:1–22.

Yang YL, Leone LM, Kaufman LJ. 2009. Elastic Moduli of Collagen Gels Can Be Predicted from Two-Dimensional Confocal Microscopy. Biophys J. 97: 2051–2060.

Zhu J, Kaufman LJ. 2014. Collagen I Self- Assembly: Revealing the Developing Structures that Generate Turbidity. Biophys J. 106: 1822-1831.

6. Appendix – Extended Tabular Data

Table 1: Average intensities of collagen monomers and fibrils from birefringence images.

Condition	Average Intensity (a.u.)	Standard Deviation (a.u.)
Control Gel	6.51	0.22
37 °C Collagen Gel	10.84	1.94
25 °C Collagen Gel	13.48	2.36

Table 2: Mean diameters of hand-measured collagen fibrils polymerized under varying polymerization temperatures and pHs calculated from SEM images.

Temperature (°C)	pH	Mean Diameter (nm)	Standard Deviation (nm)
25 (°C)	5.5	111.29	29.70
	6.5	138.27	27.43
	7.5	132.88	29.12
	8.5	91.55	29.83
37 (°C)	6.5	56.30	8.12
	7.5	102.12	9.19
	8.5	138.10	28.46

Table 3: Mean D-banding periodicity of collagen fibrils polymerized under varying polymerization temperatures and pHs calculated from SEM images.

Temperature (°C)	pH	Mean Periodicity (nm)	Standard Deviation (nm)
25 °C	6.5	54.7	6
	7.5	59.4	6
	8.5	56.0	9
37 °C	7.5	59.8	4
	8.5	61.5	7

Table 4: Mean intensity of collagen fibrils polymerized under varying polymerization temperatures and pHs calculated from segmented from SHG images.

Temperature (°C)	pH	Average Intensity (counts)	Standard Deviation (counts)
25 (°C)	5.5	269.67	90.98
	6.5	189.78	40.94
	7.5	48.14	21.56
	8.5	63.72	22.31
37 (°C)	5.5	1.35	0.95
	6.5	8.95	2.87
	7.5	14.12	7.35
	8.5	15.24	8.83